

Recent Trends in Surface Characterization and Chemistry with High-Resolution Scanning Force Methods

Clemens Barth,* Adam S. Foster,* Claude R. Henry, and Alexander L. Shluger*

The current status and future prospects of non-contact atomic force microscopy (nc-AFM) and Kelvin probe force microscopy (KPFM) for studying insulating surfaces and thin insulating films in high resolution are discussed. The rapid development of these techniques and their use in combination with other scanning probe microscopy methods over the last few years has made them increasingly relevant for studying, controlling, and functionalizing the surfaces of many key materials. After introducing the instruments and the basic terminology associated with them, state-of-the-art experimental and theoretical studies of insulating surfaces and thin films are discussed, with specific focus on defects, atomic and molecular adsorbates, doping, and metallic nanoclusters. The latest achievements in atomic site-specific force spectroscopy and the identification of defects by crystal doping, work function, and surface charge imaging are reviewed and recent progress being made in high-resolution imaging in air and liquids is detailed. Finally, some of the key challenges for the future development of the considered fields are identified.

1. Introduction

The family of scanning probe microscopy (SPM) methods employing forces for studying surface properties has developed over the last 25 years into many versatile tools in surface

physics and chemistry, as well as in nanoscience and nanotechnology. Phenomena studied by these techniques include surface topography; atomic structure; film growth; measurements of adhesion and the strength of individual chemical bonds; friction and lubrication; work functions; electrostatic, dielectric and magnetic properties; contact charging; molecular manipulation; and many others from the micrometer to the subnanometer scale. Different members of the force microscopy family specialize in different surface properties and operate in different environments and temperatures ranging from low temperatures and ultra high vacuum (UHV), to room temperatures and above, in air and in liquids. In this paper, we focus on the recent applications of two of the most commonly used techniques, non-contact atomic force microscopy (nc-

AFM) and Kelvin probe force microscopy (KPFM), to studying surfaces of insulators and thin films with atomic or nanoscale resolution. A major strength of these techniques is their lack of material restrictions, and many of the breakthrough results in high-resolution imaging have been achieved on surfaces inaccessible to other imaging techniques. The requirement of a conducting sample has long prevented studies of insulators with scanning tunneling microscopy (STM) in particular and the focus of this review on insulators has been directed by the success of force microscopy in this area. Furthermore, these materials have proven to be critical in many recent applications, such as catalysis, sensors, microelectronics, and molecular electronics.

In both nc-AFM and KPFM a sharp tip interacts with the surface and a surface image is produced by scanning. However, the forces dominating the image formation are different. In atomic force microscopy (AFM) the control parameter is the total force between the tip and sample, including the short-range interaction providing the nanoscale and atomic image contrast. KPFM is actually a suite of techniques implemented into nc-AFM, offering the measurement of local work function changes on conducting surfaces and the surface charge distribution on insulating surfaces. KPFM is dominated by long-range electrostatic forces, with short-range forces contributing to atomic contrast. In both techniques, information about the system under study is encoded in a change of these forces as the tip scans along the surface. These techniques belong to the much bigger family of SPM methods, a number of which are briefly described in **Table 1** for reference. Providing a detailed description of each of these techniques is

Dr. C. Barth, Dr. C. R. Henry
Centre Interdisciplinaire de Nanoscience de Marseille (CINaM,
The CINaM is associated with the Aix-Marseille University)
CNRS, Campus de Luminy
Case 913, 13288 Marseille Cedex 09, France
E-mail: barth@cinam.univ-mrs.fr

Prof. A. S. Foster
Department of Physics
Tampere University of Technology
P.O. Box 692, FIN-33101 Tampere, Finland
E-mail: adam.foster@tut.fi

Prof. A. S. Foster
Department of Applied Physics
Aalto University School of Science and Technology
PO Box 11100 FI-00076 Helsinki, Finland

Prof. A. L. Shluger
Department of Physics and Astronomy and the London Centre
for Nanotechnology
University College London
Gower Street, London, WC1E 6BT, UK
E-mail: a.shluger@ucl.ac.uk

Prof. A. L. Shluger
WPI-Advanced Institute of Materials Research
Tohoku University
2-1-1 Kitahira, Aoba, Sendai, 980-8577, Japan

DOI: 10.1002/adma.201002270

beyond the scope of this paper and the reader is referred to the literature cited in the table for more information.

AFM imaging is often performed in the so-called contact mode,^[1] where the tip is in constant contact with the surface, with the short-range repulsive forces being balanced by the van der Waals force or by the external elastic force of the cantilever. This technique provides a wealth of information regarding surface topography, nanotribology, and adhesion physics, but is often invasive and unreliable for imaging with true atomic resolution.^[2,3] It has been demonstrated that one can obtain a much better sensitivity in measuring force variations on the atomic scale and achieve true atomic resolution by vibrating the cantilever at a certain frequency above the surface.^[4,27] In this case, the elastic force on the cantilever overcomes the van der Waals attraction of a tip to a surface and prevents the so called “jump-into-contact”.^[2,5] Since the tip is then not in permanent direct hard contact with the surface, this technique is often also called non-contact AFM (nc-AFM). A detailed description of the technique can be found, for example, in Refs. [5–7] and an overview of applications in Refs. [1,5,7–10]. Section 2.1 briefly summarizes the nc-AFM technique.

For a long time, the classical Kelvin probe^[11,12] has been used to measure the work function of metal surfaces^[13–15] and also surface-charge-related phenomena on insulating surfaces^[16–20] with high precision in the meV range. Soon after the invention of AFM, many new scanning techniques based on measuring the electrostatic forces were introduced, such as the large family of electrostatic force spectroscopy (EFS) and electrostatic force microscopy (EFM) techniques. Inspired by classical Kelvin probe,^[21,22] KPFM is probably one of the most important types of electrostatic AFM. EFS, EFM, and KPFM differ in their function principle and are reviewed to some extent in Refs. [23,24]. In Section 3 KPFM is briefly summarized.

The rapid development and collaboration of nc-AFM and KPFM over the last few years has made them increasingly relevant for studying, controlling, and manipulating chemical species and processes at surfaces.^[8,10,25,26] In this paper we review the current status and discuss future prospects in applying these methods in combination with other surface techniques to studying individual defects, clusters, and molecules at surfaces and their interactions. We focus mainly on the recent progress and emerging trends in applying nc-AFM and KPFM in several areas of materials chemistry. In this review we cannot completely cover all the existing excellent studies and we refer an interested reader also to other recent reviews on advances in AFM for the electrical characterization of semiconductors,^[28] scanning probe microscopy of oxide surfaces,^[29–31] AFM in ambient conditions,^[32] and controlled manipulation of atoms and molecules.^[33] Although nc-AFM and KPFM are strongly interrelated in terms of the underpinning forces, and are increasingly applied together, we find it more convenient to discuss them separately.

2. Non-Contact Atomic Force Microscopy

2.1. Instrumentation

Non-contact AFM was originally based on the amplitude modulation (AM) mode,^[34] including tapping mode AFM,^[35]



Clemens Barth completed his diplomarbeit in physics at the Freie Universität Berlin (Germany) in 1999 and moved then to Munich where he obtained his Ph.D. at the Ludwig-Maximilians-Universität in 2002. After a three year postdoctoral position at the Centre Interdisciplinaire de Nanoscience de Marseille (CINaM) in France, he became a permanent researcher in the CNRS at the CINaM in 2004.



Adam S. Foster obtained his masters degree in theoretical physics at Newcastle University (UK) in 1997 and his Ph.D. at University College London (UK) in 2000. After a postdoctoral position in the Laboratory of Physics, Helsinki University of Technology (Finland), he became an Academy of Finland Senior Fellow in 2004 at the same lab. He was appointed Professor at the Department of Physics, Tampere University of Technology (Finland) in 2009.



Alexander Shluger graduated from the Latvia State University, Riga, in 1976 and received his Ph.D. and Doctor of Science degrees from the L. Karpov Physics and Chemistry Research Institute (Moscow) in 1981 and 1988, respectively. He became a Professor of Physics at the University College London in 2004. His research is focused on theoretical studies of defects in insulators and imaging and manipulation at insulating surfaces using atomic force microscopy.

where the cantilever is excited at a fixed frequency with constant amplitude (constant excitation mode). Upon approach to the surface, the tip–surface interaction causes a change in the amplitude and phase of the cantilever oscillations, providing a measurable signal, which is used to regulate the tip–surface distance. In practice, the response of the cantilever in this mode was found to be rather slow for UHV applications,^[6] and it was replaced by the frequency modulation (FM) mode^[6] in atomic

Table 1. Key features of different high-resolution SPM techniques. Terms such as electrostatic modulation/contribution and 1st and 2nd harmonic are explained in Section 3. More details about each technique can be found in the selected references. Note that the references are only a part of the whole literature. For a complete understanding of the techniques, the reader should also study the literature, which is cited or cites the references in the table.

Base Technique	Mode	Dynamic	Characteristics/Notes	Feedback for tip–surface distance	Measured signals, images	Typical tip–surface distance (nm)	Literature
Scanning Tunneling Microscopy	STM	No		Tunneling current	Topography	0.6–1.0	[9, 326, 327]
Atomic Force Microscopy	Contact (c-AFM)	No		Cantilever deflection (normal force, F_N)	Topography, lateral force	short-range, repulsive tip–surface interaction	[1, 2, 369]
	Amplitude modulated nc-AFM (AM nc-AFM)	Yes	Constant excitation at constant frequency	Amplitude, A , or phase, ϕ	Topography, dissipation	1.0–5.0	[6, 7]
	Frequency modulated nc-AFM (FM nc-AFM)	Yes	2 nd loop for constant amplitude regulation	Frequency change, Δf	Topography, dissipation	0.3–5.0	[5, 6, 7]
	Tapping mode AFM	Yes	In principle, AM nc-AFM with very large amplitudes, tip–surface contact	Amplitude, A , or phase, ϕ	Topography, dissipation	Short-range, repulsive tip–surface interaction	[35]
	Constant height mode AFM	Yes/No	Can be applied either in c-AFM or AM/FM nc-AFM	None or very slow feedback on F_N (c-AFM), Δf (FM nc-AFM), or A (AM nc-AFM)	F_N (c-AFM), Δf (FM nc-AFM), or A (AM nc-AFM) + dissipation in nc-AFM	0.3–5.0	[36, 37, 38]
Electrostatic Force Spectroscopy (EFS)	Spectroscopy	Yes	Dependence on voltage or time or distance; Electrostatic modulation can be applied	No feedback, the tip is fixed above the surface	nc-AFM signals (Δf or A , dissipation) or 1 st harmonic of the electrostatic contribution	0.5–5.0	[370, 305, 314, 380]
Electrostatic Force Microscopy (EFM)	Normal topography imaging in nc-AFM; Single-pass method	Yes	The image evolution is observed either in dependence on time or voltage, from image to image	nc-AFM feedback	Piezo elongation in z (topography signal)	1.0–5.0	[302, 370, 371, 372]
	Double-pass mode	n.a.	After a topography image or scanning line has been obtained, the tip is placed at a distance of 10–100 nm above the surface for electrostatic force detection of the same surface area	No feedback	Either detuning Δf or phase, ϕ , of the cantilever resonance frequency or 1 st harmonic of the electrostatic contribution	10–100	[23, 373]
	Single-pass mode	Yes	Normal nc-AFM imaging + electrostatic modulation	nc-AFM feedback	1 st and 2 nd harmonic of the electrostatic contribution	1.0–5.0	[374, 375, 376]
Scanning Polarization Force Microscopy (SPFM)	Single-pass mode	Yes	The 2 nd harmonic of the electrostatic contribution is used for the tip–surface distance regulation (FM and AM nc-AFM)	2 nd harmonic of the electrostatic contribution	1 st harmonic of the electrostatic contribution and piezo elongation in z (topography signal)	1.0–5.0	[377, 378, 379]
Kelvin Probe Force Microscopy (KPFM)	Frequency modulation, single-pass mode	Yes	The frequency of the electrostatic modulation is much smaller than the cantilever resonance frequency, typically < 5 kHz	nc-AFM feedback + Kelvin loop	Tip–surface contact potential difference	Normal distance: 1.0–5.0 (atomic resolution closer)	[294, 296, 297]
	Amplitude modulation, single-pass mode	Yes	The frequency of the ac voltage is mostly put onto the 1 st harmonic of the cantilever oscillation (6.3 x cantilever resonance frequency)	nc-AFM feedback + Kelvin loop	Tip–surface contact potential difference	Normal distance: 1.0–5.0 (atomic resolution closer)	[295, 296, 297]

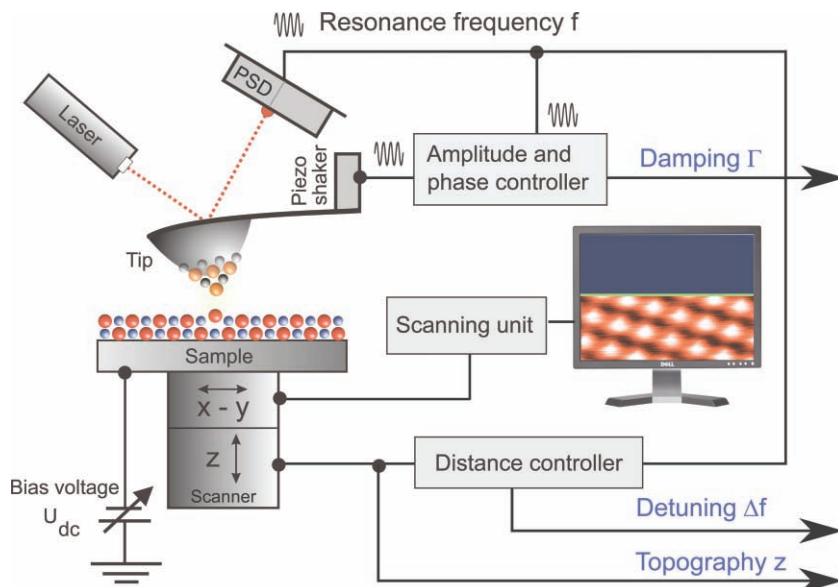


Figure 1. Schematic setup of a frequency modulation nc-AFM, consisting of two independent regulation loops. The amplitude/phase controller keeps the amplitude of the cantilever oscillation constant, whereas the distance controller adjusts the tip–surface distance by keeping the detuning Δf at a constant value. The damping or dissipation output reflects the energy required to maintain a constant amplitude of the cantilever oscillation, and can also be used as an imaging signal.^[8,9] Note that the drawing is only a simplified diagram of the function principle. More details can be found, for example, in Ref. [39].

resolution studies. However, the AM mode and tapping mode AFM have proven rather successful in air and liquids^[7] (see Section 2.9). In FM mode, a nc-AFM cantilever is maintained in oscillation at a constant amplitude via a feedback loop (constant amplitude mode) and can be considered as a self-driven oscillator (**Figure 1**). If there is an interaction (force) between the tip and surface, the cantilever resonance frequency changes from f_0 to a new frequency, f , which strongly depends on the tip–surface distance. The detuning is therefore the main signal in FM nc-AFM and is used for the tip–surface distance regulation. The distance is mostly regulated upon changes in the detuning, Δf , which is kept constant on a pre-set value, $\Delta f_{\text{pre-set}}$, by a second feedback loop, and the resulting topography map provides the image of the surface. It is also possible to image at quasi-constant height, where the change in Δf provides the imaging signal.^[36–38]

Traditional nc-AFM applications in surface science, such as the research on surface structure analysis, surface reconstructions, surface growth, surface dynamics, and surface chemistry, are carried out implementing the FM mode in UHV chambers with pressures of less than 10^{-9} mbar. Aside from the sensitivity benefits for nc-AFM, this is mainly to keep the surfaces clean for as long as possible. For biological applications, e.g., the research of DNA and single cells, as well as for electrochemical purposes, AFM can be operated under liquid conditions.^[25,40–48] Until recently, operating in a non-UHV environment substantially limited the spatial resolution. However, technical advances in improving the sensitivity of AFMs provided by operating at small cantilever amplitudes^[49] have opened the door to molecular and atomic resolution in liquids, air, and ambient gases^[32] (see Section 2.9).

The recipe for preparing the surface before scanning varies with the specific material and successful approaches are normally found by trial and error. Although AFM can, in principle, handle any topography, large changes in force gradient over particularly rough patches on the surface result in oscillation instabilities because the feedback electronics cannot react quickly enough. Hence, the surface itself must be relatively flat (almost atomically) and “clean” for high-resolution scanning. Sputtering and annealing in controlled cycles and in different conditions is often used on metal and oxide surfaces to get rid of surface contaminants and to prepare stoichiometric or reduced surfaces. A majority of insulating surfaces can be prepared by cleavage, sometimes resulting in a high density of defects and “rubble” on the surface, as in the case of MgO(001).^[50] The main problem on insulating surfaces (and on undoped semiconductors) is localized charges at or near the surface, resulting from cleavage, sputtering, and/or formation of space charge. These charges cause significant long-range electrostatic forces, making scanning more difficult by reducing the relative contribution of short-range forces and increasing the possi-

bility of tip crashes. Reducing the effect of electrostatic forces can be achieved by minimizing Δf as a function of the applied bias between the tip and a certain point on the surface^[51] or by specific surface preparations techniques such as annealing.^[50,52] For conducting surfaces or insulating thin films, the application of bias also compensates for the work-function difference between the tip and surface by reducing long-range capacitive forces. The role of bias in AFM will be discussed in more detail in relation to KPFM in Section 3.

The tip is the most important element in high-resolution AFM studies, yet tip preparation remains an art rather than science. In most cases, the tip and cantilever are fabricated as a single structure by etching silicon in very much the same way as semiconductor chips. Since, regardless of the operating conditions, the tip is exposed to the ambient atmosphere, it is originally oxidized and at least partially hydroxylated.^[53] It is possible to use these hydroxylated silica tips if great care is taken during scanning, but this appears to give poor resolution due to weak interaction with the surface.^[54] In some experiments sputtering and/or annealing are then used to attempt to clean the tip. Another increasingly popular tip fabrication route is to use a quartz tuning fork as the cantilever, separately glueing a tip to the fork^[55,56] (see Section 2.9).

Regardless of the fabrication route chosen, for high-resolution studies, it is the nature of the very end of the tip that is crucial. To achieve control over the tip apex atomic structure, attempts have been made to produce clean silicon tips,^[57] even with specific orbital configurations at the apex,^[58] but no images have yet been produced with these tips on anything other than silicon surfaces. Metal-coated and metallic tips have also been used in numerous studies,^[59–65] but establishing the real structure

of a tip apex remains challenging and evidence of real control over tip structure is still lacking. In some cases the tip was modified by controlled adsorption of molecules^[66,67] or even carbon nanotubes,^[68–70] but while these offer improvements in stability for lower-resolution imaging, they have not yet been routinely successful for high-resolution studies. Even if the last atom of the tip can be identified, it has to be guaranteed that the tip does not change during an AFM measurement. Tip changes, however, appear regularly during scanning until the chemical potential equilibrium between tip and sample is (at least temporarily) formed. Therefore the chemical composition of the last atoms of the tip is extremely difficult to control. This is why tips are often purposely brought into contact with the surface, in an attempt to facilitate establishing such an equilibrium, with the hope that a sensitive, but also stable, nanotip is formed.

Recently, metallic tips functionalized by adsorption of Cl atoms and CO molecules have been used successfully to resolve the atomic structure of pentacene and other molecules adsorbed on NaCl films on Cu(111).^[64] This approach provides a potential route to achieve a degree of control over the tip structure, but it has been implemented so far only using a combined STM/AFM instrument at low temperature in a system featuring thin NaCl islands on a metal surface. This allowed picking up atoms and molecules in a controlled fashion from the metal surface using the instrument in the STM mode of operation. The applicability of this technique to a wider variety of substrates has yet to be demonstrated.

2.2. Methods and Challenges in Interpretation of nc-AFM Images

The overall strength of the interaction between tips and surfaces is mainly determined by long-range van der Waals and electrostatic forces. However, the atomic contrast in nc-AFM images is dominated by short-range van der Waals, electrostatic, and covalent interactions between the tip apex and the atoms in the surface.^[7,9,71,72] It is an over-simplification to consider this to be equivalent to a single atom at the apex interacting with a single atom in the surface, although the closest tip–surface pair often dominates the interaction. The real interaction at every point in an AFM scan will include all atoms in the tip and surface, augmented by any associated tip- and surface-atom relaxations. In practice, this means that the contrast measured is very sensitive to the nature of the tip.

As an example, in the FM nc-AFM studies of the silicon surface,^[4] the complex reconstruction of the surface and the identical chemical composition of both tip and sample initially prompted fairly straightforward interpretation of experimental images. Assumptions that the contrast was mainly determined by a silicon dangling bond at the

tip apex interacting with silicon in the surface were qualitatively confirmed in later theoretical and experimental studies.^[72,75,76] However, further investigations showed that this agreement is not always valid and that, for example, an oxidized tip provides a very different contrast pattern on silicon.^[54] The early Si tip models were also shown to be too simplistic and more sophisticated models were later proposed.^[77] In fact, silicon has become the exception that proves the rule that interpretation in AFM is not possible from a single experimental image alone. Most samples of interest contain at least two different species and assigning the measured contrast pattern, or patterns, cannot be done by eye. It usually requires a systematic combination of experiment and theory, the nature of this combination has been very system dependent, and no universal approach has been discovered yet.

Since AFM is very sensitive to short-range chemical interactions, an obvious extension beyond imaging is to directly measure the forces over specific sites on the surface, so-called force spectroscopy (see **Figure 2a,b**). This proved to be extremely challenging experimentally due to the necessity to greatly reduce sources of noise in order to maintain the position of the tip over a given site on the surface and measure the force to a useful accuracy. Low-temperature AFM was introduced as a general method for improving the sensitivity and controllability of experiments,^[78,79] with operating temperatures down to below 10 K. This proved to be the essential step in the development of force

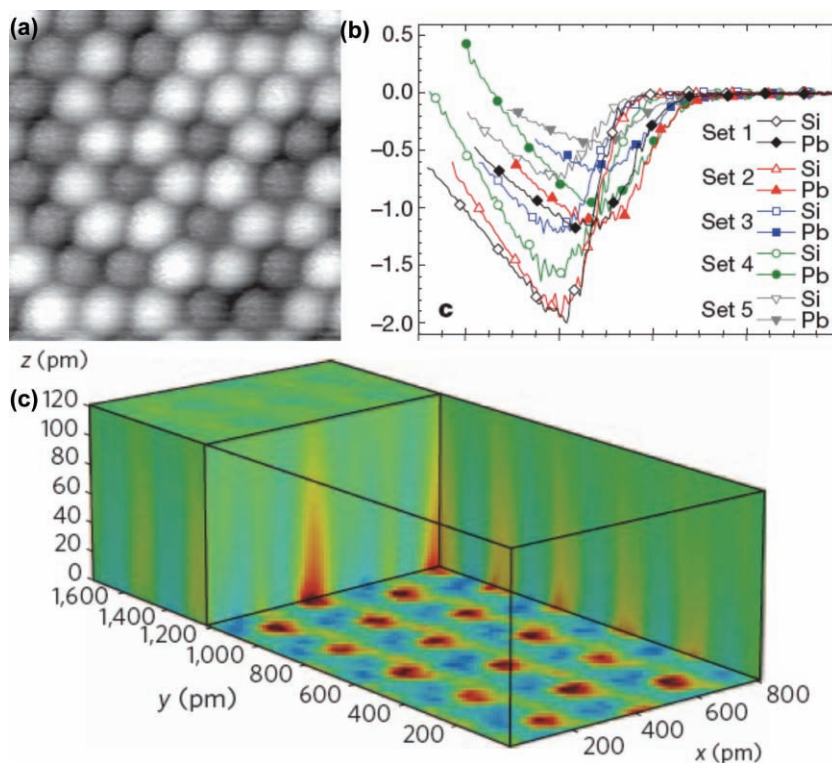


Figure 2. a) High resolution nc-AFM image of a mixture of Sn, Pb and Si atoms on the Si (111) surface and b) sets of force curves measured over Pb and Si atoms. The discrimination between the different atomic species could be accomplished by comparing experimental and theoretical force spectroscopy. c) 3D force spectroscopy of the graphite surface. Panels (a,b) reproduced with permission.^[73] Copyright 2007, Nature Publishing Group. Panel (c) reproduced with permission.^[74] Copyright 2009, Nature Publishing Group.

spectroscopy and nearly all successful measurements were at low temperature.^[59,75,76,80–82] The recent introduction of atom-tracking software, made obtaining force spectroscopy at room temperature also possible, greatly increasing its accessibility,^[83,84] with results demonstrating resolution comparable to the best low-temperature studies.^[73] Recent developments in controlling drift of the tip offer the promise that similar levels of control can also be achieved at room temperature in air^[85] and liquids.^[86]

Having achieved force spectroscopy over specific surface sites, it seems natural to attempt an atom-resolving, 3D imaging mode (see Figure 2c). This requires measuring densely spaced force curves suitable for producing high-quality force maps along any plane parallel or perpendicular to the surface. However, combining thousands of $\Delta f(z)$ curves to form a 3D data set that allows the recovery of forces and energies is not straightforward. This requires long acquisition times and overcoming problems of drift and tip stability. Since the first measurements on the NiO (001) surface^[59,80,87] significant progress has been made in this area both in UHV^[88] and in solution.^[86]

Force spectroscopy can greatly aid image interpretation because it is relatively easy to calculate force curves over a few sites in the surface for comparison to the measured curves, even with state-of-the-art first-principle simulations.^[7,9] To calculate an image or 3D force map, tens of thousands of points are often needed and significant approximations need to be made in the calculation methodology to make the simulations feasible. In contrast, simulations of several force spectroscopy curves can be made with state-of-the-art quantum mechanical calculations, leaving the main uncertainties in the nature of the system itself. Early successes provided good agreement between measured and calculated force curves,^[76,81,82,89] while also highlighting, as expected, the sensitivity of the force curves to the exact tip structure and chemistry. Comprehensive comparison between experimental and theoretical force curves, and hence comprehensive interpretation, often requires calculating a large set of possible tip models,^[89,90] measuring enough experimental curves to provide meaningful statistics,^[73] or achieving qualitative or semi-quantitative agreement in curve characteristics.^[81,82]

For conducting samples, combining nc-AFM and STM offers both current and force as local maps of the surface, reducing the free parameters in interpretation. This can be particularly powerful if contrast in one of the modes is already understood from simulations and can be used as a reference for the other mode. The approach was first used to study molecular adsorption on TiO₂ (110),^[91] then later with simultaneous force and current measurements, again on TiO₂ (110),^[92] and also for detailed current and force spectroscopy on graphite.^[93] Recent studies of molecular manipulation on metal surfaces have also used STM for spatial characterization while FM nc-AFM provided force measurements.^[62] In Section 2.5 an example illustrating how the combination of AFM and STM, along with other approaches, has been used to study the TiO₂ (110) surface is given.

2.3. Insulating Surfaces

For some systems, the surface symmetry permits the different measured contrast patterns to be immediately attributed to

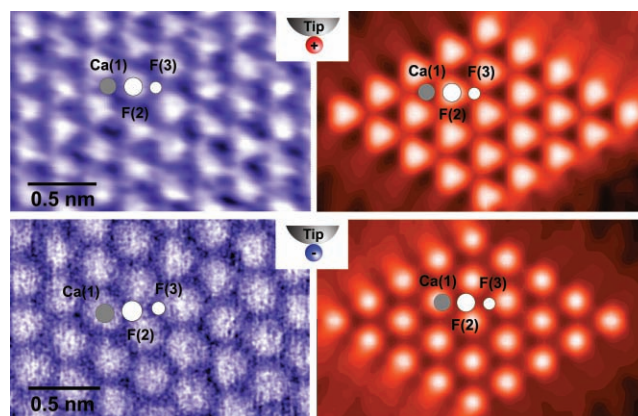


Figure 3. Comparison of experimental (left) and simulated (right) nc-AFM images of the CaF₂ (111) surface. The images show the contrast for a positive (top) and negative (bottom) potential tip. A negative potential tip interacts most strongly with the Ca²⁺ ions in the surface, resulting in a disk-like contrast. A positive potential tip interacts with both F⁻ ionic sublattices resulting in a triangular contrast. Top panels adapted with permission.^[94] Copyright 2001, American Physical Society. Bottom panels reproduced with permission.^[95] Copyright 2002, Institute of Physics.

certain types of tips. This requires an initial simulation effort to interpret the original set of contrast patterns, but then acts as a reference for interpretation of all future experiments. The first example of this is the CaF₂ (111) surface, where it has been demonstrated that tips of negative electrostatic polarity give disk-like contrast patterns with Ca²⁺ ions as bright and tips of positive electrostatic polarity give triangular contrast patterns with F⁻ ions as bright^[36,94,95] (Figure 3). This understanding of the contrast pattern was then used to interpret further AFM experiments on molecular overlayers,^[96] water adsorption and manipulation,^[97–100] thin films,^[101] and force spectroscopy.^[82] Other images of the CaF₂ (111) surface were obtained using the qPlus sensor technique of nc-AFM with an etched tungsten tip, and they exhibited the step edges and screw dislocations expected following in situ cleavage in UHV.^[102] Another result of this latter work was that the atomically resolved images obtained using a small-amplitude mode with a tungsten tip also exhibited disk-like and triangular contrast features. This indicates that in both cases tips were terminated by polar clusters, likely due to contamination by surface material. Si tips intentionally contaminated by surface material via hard contact with the cleaved CaF₂ (111) surface were used to image a perfect surface and point defects.^[97,99] Again the two distinct types of contrasts were observed, corresponding to two different tip polarities. Based on the observed defect images and defect mobility the authors concluded that the positively charged hydrogen ion of the H₂O molecule occupying a Ca²⁺ site in the surface is likely to be the point defect observed in the study (Figure 4a,b).

Similar studies have been carried out on the CeO₂ (111) surface, which has the same structure as the CaF₂ (111). CeO₂ (111) is used in a variety of industrial applications, such as catalysis, fuel cells, and oxygen sensing, due to its high oxygen transport and storage capacities and studying surface defects is vital for understanding these properties. However, contrary to initial expectations, the atomically resolved images of the CeO₂ (111)

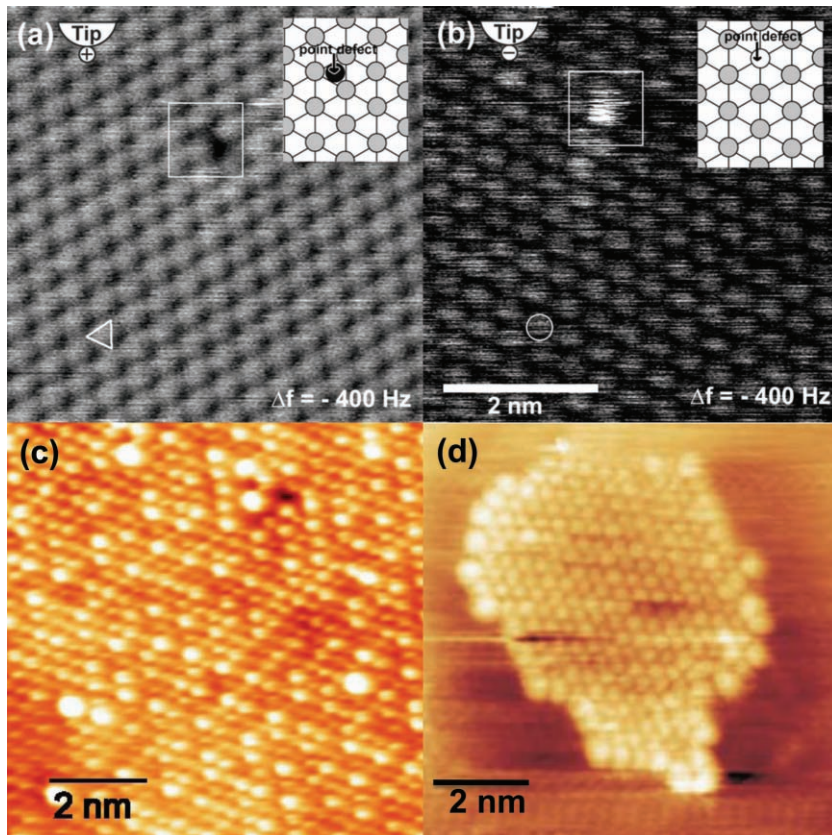


Figure 4. Examples of nc-AFM images with atomic resolution. The CaF_2 (111) surface and a point defect imaged with a) a positively terminated and b) a negatively terminated tip. The CeO_2 (111) surface c) slightly reduced and d) with a small surface island formed during annealing. Panels (a,b) adapted with permission.^[99] Copyright 2007, Institute of Physics. Panel (c) adapted with permission.^[103] Copyright 2007, American Physical Society. Panel (d) adapted with permission.^[104] Copyright 2008, American Institute of Physics.

surface, obtained by many sputter/anneal cycles of crystalline samples, exhibited predominantly disk-like contrast.^[105,106] Only occasionally have other types of contrast, e.g., a honeycomb pattern, been observed.^[107] This made the chemical identification of image features more difficult than for the CaF_2 (111) surface,

where two contrast patterns gave rise to an unambiguous interpretation. The reason for this difference is still unclear and may have to do with the way CeO_2 contaminates Si tips upon repeated contact. However, unlike the CaF_2 (111) surface, CeO_2 (111) proved to be a playground for a wide variety of point defects that are stable at room temperature.^[103,105,106,108] Plausible models have been suggested for chemical identities of image features and defects; these have been used to understand the interaction of water with the surface^[105,109] (Figure 4c) and the structure of steps at surfaces observed with atomic resolution^[104,106] (Figure 4d). However, full understanding of the surface chemistry and interpretation of images remains a challenge.

More generally, the improving ability of FM nc-AFM for studying a wide variety of insulating surfaces in high resolution can be seen in recent successes in resolving long-standing issues in structural characterization, particularly on those materials inaccessible to other surface probe techniques (Figure 5). Some pertinent examples include diamond,^[115] and binary oxides, such as MgO (001)^[110] and bulk $\alpha\text{-Al}_2\text{O}_3$ (0001).^[111,116] There has also been recent progress in imaging polar oxides, such as ZnO (0001),^[113,117] and minerals, such as mica,^[112,118] antigorite,^[114] and calcite (10–14).^[119]

2.4. Doping Samples

As discussed in Section 2.2, the interpretation of chemical atomic contrast is never straightforward. It is particularly difficult for binary insulators, such as NaCl or MgO , where the cations and anions are arranged in equivalent cubic sublattices on the (001) surface. In this case, images with atomic resolution exhibit the same type of contrast, which

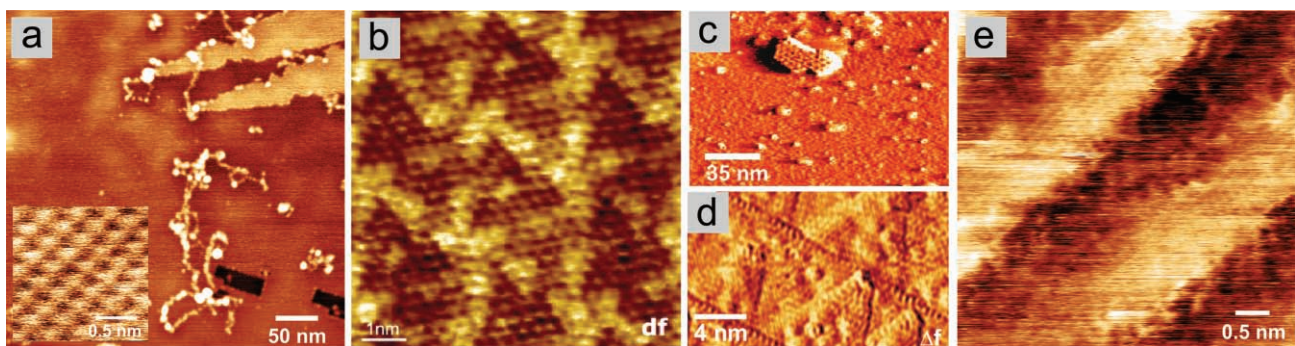


Figure 5. nc-AFM high-resolution images of a) MgO (001) (inset shows the atomic resolution on flat terraces), b) bulk $\alpha\text{-Al}_2\text{O}_3$ (0001), c) potassium carbonate islands on mica, d) ZnO (0001), and e) antigorite ($(\text{Mg,Fe,Al})(\text{Si,Al})\text{O}(\text{OH})$). Panel (a) adapted with permission.^[110] Copyright 2003, American Physical Society. Panel (b) adapted with permission.^[111] Copyright 2009, American Physical Society. Panel (c) adapted with permission.^[112] Copyright 2009, American Chemical Society. Panel (d) adapted with permission.^[113] Copyright 2008, American Physical Society. Panel (e) adapted with permission.^[114] Copyright 2010, American Mineralogical Society.

is nearly always composed of round bright and dark disks, independent of the composition of the tip.^[120–123] Identifying these contrast features requires extensive experimental and theoretical effort, such as comparison between experimental and simulated images or force spectroscopy (see Section 2.2).

A very promising approach to interpreting images of such crystal surfaces is to dope them with known impurities, which is a general experimental method that has been used effectively for studying defects in bulk crystals for many decades.^[124–126] The adsorbates or impurities present on the surface are likely to exhibit different atomic contrast in comparison to the rest of the surface ions,^[127] hence identifying an impurity aids significantly in also identifying all other types of ions at the surface. This labeling was shown by early experiments on surfaces of mixed $\text{KCl}_{0.6}\text{KBr}_{0.4}$ crystals.^[122] Despite the similarity of formal charges, the Cl^- , Br^- , and K^+ ions could be identified.

However, doping crystals with aliovalent impurities has more advantages because such impurities exhibit a clear difference in the atomic contrast with respect to all other regular ions.^[127] A benefit is that the inclusion of aliovalent impurities may lead to a restructuring of the ions locally in the bulk and also on the surface. A new phase can be created with a different crystal lattice, which is usually accompanied by the introduction of vacancies or interstitials compensating for the adifferent charge of the aliovalent impurities.^[128] For instance, if an alkali halide crystal is doped by a relatively large amount of divalent metal ions (1–10%), the impurities and cation vacancies aggregate into the Suzuki phase.^[129] The main characteristic of the Suzuki phase is that the lattice vectors of its cubic structure are twice as long as those of pure NaCl and that the phase is formed from ordered cation vacancies and impurities.^[129–131] In doped NaCl crystals, the Suzuki phase can be found in large precipitates, which have a cubic shape^[132] and are almost perfectly embedded into the NaCl matrix. Cleaving and additional annealing in UHV leads to the segregation of impurities and vacancies to the surface^[133] and to a complete reconstruction of the surface.^[134] The (001) surface, which is called a Suzuki surface in the following, is nanostructured such that the two types of atomically flat surface regions coexist: pure NaCl regions and Suzuki phase regions^[134] (Figure 6a).

The surface of a Suzuki precipitate can be terminated either by a layer of pure NaCl (Figure 6c) or by a defect-rich NaCl layer, which includes the Na^+ vacancies and impurity ions (M^{2+}) in a highly ordered arrangement (Figure 6b). The results obtained on NaCl:Mg (001) surfaces^[135] demonstrate that each single ionic species can be identified directly in the image due to the different atomic sublattices of the Suzuki structure, which all have different geometries. A recent quantitative comparison between experiment and theory strongly supports this identification of all ions on the (001) surfaces of NaCl:Mg²⁺ and NaCl:Cd²⁺ crystals.^[136] This identification can be done independently of the tip–surface distance and despite differences in surface termination. It does not depend on the chemical nature of the divalent impurity ions inside the Suzuki structure.^[136]

This work opens up an interesting prospect for controlling surface chemistry by the choice of impurity. For instance, the Suzuki phase is known to be formed in NaCl by other divalent ions (e.g., Mn^{2+} ,^[137,138] Fe^{2+} ^[130]) as well as in other host lattices,

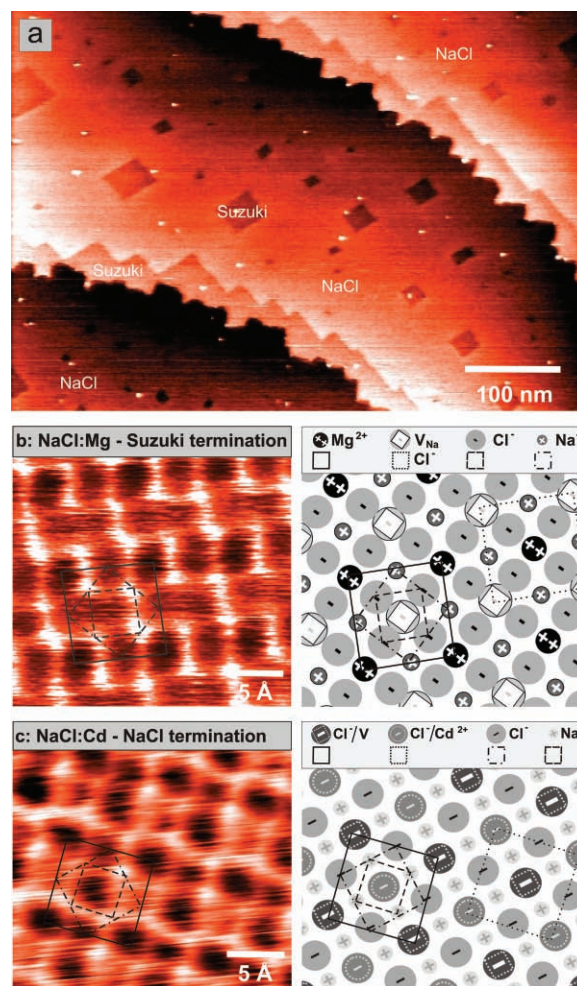


Figure 6. The (001) Suzuki surface of NaCl-doped crystals. a) Large-scale image representing the nanostructured Suzuki surface. The surface is composed of pure NaCl regions and precipitates condensed in the Suzuki phase ($\text{NaCl}:\text{Cd}^{2+}$). b) Experimental image of the $\text{NaCl}:\text{Mg}^{2+}$ surface, terminated by the layer including all impurities and vacancies. c) Experimental image of the $\text{NaCl}:\text{Cd}^{2+}$ surface, terminated by a pure NaCl layer. In both experimental images, all ions can be identified due to the individual sublattices formed either by the Cl^- , Na^+ , $\text{Mg}^{2+}/\text{Cd}^{2+}$, or vacancies (V) (compare with drawings). For a detailed description of the atomic contrast see Refs. [134–136].

such as $\text{LiCl} (: \text{Mg}^{2+}, \text{V}^{2+}, \text{Mn}^{2+})$,^[139] $\text{LiF}:\text{Mg}^{2+}$,^[140] $\text{MgO}:\text{Mn}^{4+}$, and $\text{NiO}:\text{Mn}^{4+}$ ^[141,142]. An interesting challenge would be to create a Suzuki phase incorporating magnetic impurities, such as Mn^{2+} and Fe^{2+} ^[137]; magnetic ordering in these structures could be studied by magnetic exchange force microscopy.^[60] Another application of this approach could be in nanocatalysis, where oxides such as MgO, are used as supports for metal nanoclusters.^[143,144] As $\text{MgO}:\text{Mn}^{4+}$ ^[141] and $\text{NiO}:\text{Mn}^{4+}$ crystals^[142] exhibit Suzuki precipitates, such systems could allow both identifying the surface ions and tailoring catalytic properties.

Using the Suzuki surface for identifying ions in nc-AFM images could also help in studying deposited nano-objects, such as molecules and metal clusters. A possible scenario is that ions in the Suzuki structure and the polarity of the tip are

first identified. This information can then be used to characterize the chemical contrast of supported nano-objects and to provide a clear system setup for numerical simulations. A further benefit is that the impurity ions and vacancies can serve as anchoring sites for the nano-objects.

From a more general perspective, the example of the Suzuki surface clearly shows that doping may become one of the standard procedures in nc-AFM. Indeed, a recent application using nc-AFM spectroscopy for identifying dopants in the Si(111) surface (see Figure 2) demonstrates the feasibility of this approach.^[73] Further evidence that doping becomes an important procedure can be seen in recent measurements on oxide surfaces, such as TiO₂ (110),^[145,146] where high-resolution images offer some insight into the role of dopants in photocatalytic processes on the surface.

2.5. Combining STM and nc-AFM: the TiO₂ (110) Surface

The importance of titanium dioxide (TiO₂) in a wide variety of applications ranging from photocatalysis to biomedical implants^[147–150] has led to a considerable research effort to understand its surface properties.^[151] The most stable (110) rutile surface is characterized by rows of oxygen atoms bridging titanium ions. Although in principle it is an insulator, TiO₂ has a small band gap (3 eV for the stoichiometric surface) and is thus accessible to both STM and AFM. Atomic resolution has been achieved on the (110) surface in both STM^[152] and AFM.^[153,154] For STM, the contrast in images was understood through extensive cooperation between theory and experiment, identifying Ti atoms as the bright sites.^[152] In AFM, images of the TiO₂ (110) surface^[92,153,154] were initially interpreted based on the concept that the force between the tip and sample was largely element independent, and therefore the protruding oxygen rows should appear as bright because they are closer to the tip. However, the tip proved to be the key to understanding and interpreting experiments on the TiO₂ (110) surface. The early AFM simulations using a hydrogen-terminated, one-atom Si tip^[155] supported the interpretation of oxygen as bright in images, but more extensive works, considering three different tip models interacting with both the ideal and vacancy-defective surfaces, predicted strongly tip-dependent imaging.^[156–158] Indeed, the experimental contrast pattern could be reproduced with a larger silicon tip, as well as with both O- and Mg-terminated MgO tips. For the O-terminated tip, the contrast was reversed with respect to the other tip models and the titanium ions were imaged as bright. Although these calculations confirmed the belief that oxygen vacancies would be seen as dark on bright

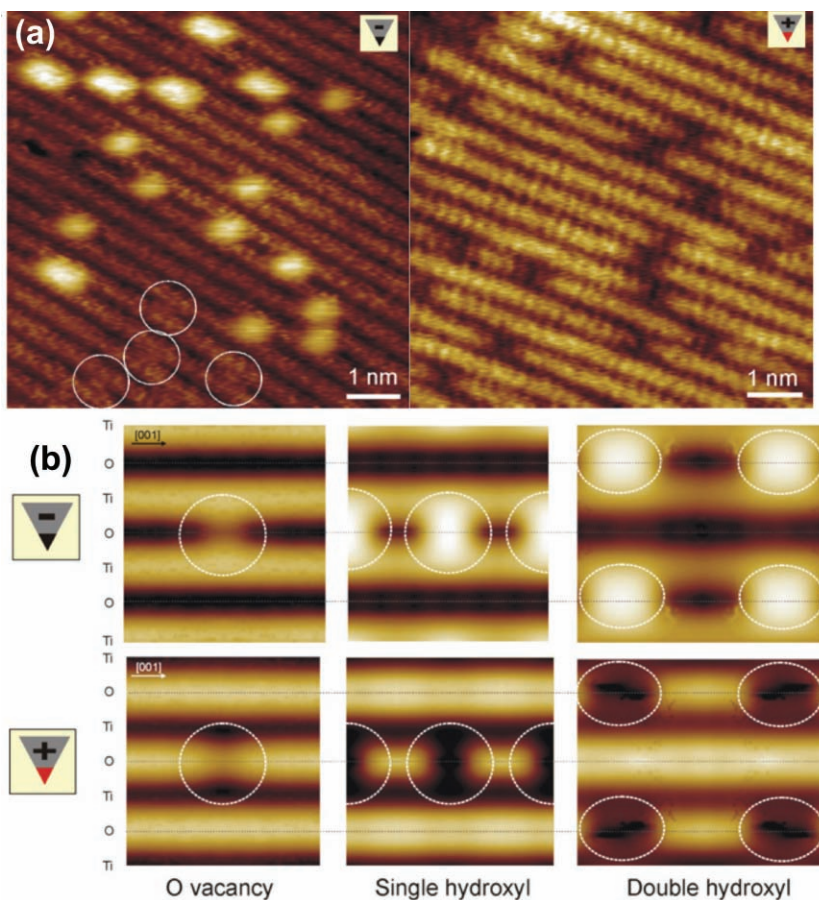


Figure 7. Comparison of experimental (a) and simulated (b) nc-AFM images of vacancies and hydroxyl species on the TiO₂ (110) surface. The triangular icon indicates the electrostatic potential of the tip. For a positive-potential tip the bridging oxygen rows are imaged as bright rows, while vacancies and hydroxyl groups are imaged as dark spots on the rows. For a negative-potential tip, the in-plane titaniums are imaged as bright rows and vacancies and hydroxyl groups are imaged as bright spots in-between the rows. Adapted with permission.^[159] Copyright 2006, Institute of Physics.

oxygen rows for a silicon tip, this was not a general result for all tips.

A much more complete picture was found by using the knowledge of water chemistry on the surface provided by STM^[160] as a background for FM nc-AFM studies. This established that the surface is always partially reduced after preparation, but soon, even in UHV, ambient water molecules begin to dissociate at the oxygen vacancies resulting in hydroxyl groups. Extensive AFM experiments could clearly distinguish three statistically significant defect species in atomically resolved images,^[159] and these defects could be seen in two reproducible imaging modes (Figure 7). One mode, called “hole”, resolved the defects as dark spots on bright rows, while the other mode, called “protrusion” resolved the defects as bright spots in-between rows. Simulations showed that both of these modes could be explained by the apex of the AFM tip exposing either a positive or negative termination. They unambiguously defined the ionic sublattices and revealed the exact positions of oxygen vacancies and hydroxyl (OH) defects on the TiO₂ (110) surface. In an extended study,^[161] a third, and rarer, “neutral” mode

was introduced, which appeared to image the physical topography of the surface and defects. This contrast pattern was suggested to be due to a clean silicon tip. Understanding of AFM imaging of the TiO₂ surface was further expanded by a detailed comparison of experiments and first principles calculations, which showed that it was even possible to see both bridging oxygens and surface titaniums as bright in images with the appropriate tip.^[162]

In contrast to the trend of using STM understanding to aid in interpretation of AFM on TiO₂,^[91,92,154,159] combined STM/AFM studies^[163] actually used the interpretation provided by AFM^[159] to understand STM images. In these latter studies, the experiments were regulated on the frequency change of the oscillating cantilever (nc-AFM), while the average current during an oscillation was measured (STM). This means that the tip was much closer to the surface than in conventional STM experiments and played a much more significant role in contrast formation in both the topography and current channels. A wide variety of experimental images were observed, with bright contrast in STM and AFM both in-phase, i.e., on the same atomic rows, and out-of-phase. Regardless of whether the tip was imaging in hole, protrusion, or neutral AFM modes, there was no general correlation between the contrast observed in the nc-AFM and the STM modes. The exact state of the SPM tip must therefore be determined for each specific case. This was achieved by carefully evaluating the STM contrast from a fairly large library of SPM tips and linking it to the appropriate nc-AFM imaging mode. For each set of experimental images, the tip was clearly defined by an exclusive match to paired AFM and STM contrast patterns and the contrast in AFM and STM was fully understood.^[163] Although the initial study provided only qualitative agreement between simulations and experiments, this was later extended to quantitative agreement by a careful consideration of the exchange-correlation functional used in calculations and inclusion of the effects of tip-surface relaxations and impurities.^[164]

The power of this approach was further demonstrated by its ability to resolve and interpret an event that neither technique could manage alone.^[165] Time-resolved nc-AFM images showed the disappearance of a single hydroxyl species during scanning. However, the average current channel showed that the signal from hydroxyl had not disappeared and had just changed slightly in position and appearance. Using the library of reference tips from earlier studies,^[163] simulations were able to identify a suitable tip to match the AFM and STM contrast. This was then used to prove that the hydroxyl group had been manipulated into a subsurface site, completely screening it from detection via force, but remaining a perturbation in the electronic structure and the corresponding tunneling current. The study of the TiO₂ (110) surface demonstrates that combining STM with AFM and extensive simulations adds extra strength to these local techniques. The recent success in high-resolution KPFM studies^[166] shows that this approach can be expanded to a wider selection of SPM flavors.

2.6. Thin Insulating Films on Metals

Another system class accessible to both STM and nc-AFM is of ultrathin insulating films grown on conducting surfaces. Thin-film systems are used in different technologically important fields, such as catalysis, spintronics, and molecular- and microelectronics.^[167–169] The simplest thin-film systems are alkali-halide films, which can be studied by STM^[170–174] and nc-AFM,^[64,65,121,175] or CaF₂ films.^[101] More relevant systems for catalysis are thin oxide films, which have been extensively characterized. A particularly well-studied example is MgO (STM^[176,177] and nc-AFM^[178–180,324]).

For all types of thin-films, the collaboration of AFM and STM is quite fruitful, and this can be best seen in the case of ultrathin Al₂O₃ films due to their interesting nanostructuring. Two types of Al₂O₃ films have been studied extensively but, so far, separately by STM and nc-AFM. The first type of film is grown on NiAl (110),^[181] whereas the second type is grown on the Ni₃Al (111) surface.^[182] The atomic structure of Al₂O₃/NiAl (110) films has been studied first by STM,^[183,184] but recently also by nc-AFM.^[63,185] The combination of structural information obtained from STM and from DFT calculations facilitated the determination of the true atomic structure of this film.^[184] The results from nc-AFM strongly supported the model so that an overall complete picture of the atomic structure could be obtained.^[63]

On the Al₂O₃/NiAl (110) surface defects are randomly distributed, resulting in an irregular array of clusters, which have a broad size distribution.^[167] Contrary to this film, the surface of alumina on Ni₃Al (111) is nanostructured in a way that promotes growth of a regular array of metal nanoclusters with a sharp size distribution.^[186] On the clean Al₂O₃/Ni₃Al (111) surface, STM reveals two hexagonal superstructures with the lattice parameters of 4.1 and 2.4 nm, which are observed at two specific bias voltages and which can be observed, for example, within two separate images.^[187] On the contrary, nc-AFM shows these two superstructures coexisting in one image, suggesting that their origin is not a purely electronic effect (**Figure 8**).^[188,189] Images reveal that the top-most atomic layer is modulated with periods corresponding to the two superstructures observed earlier by STM. The origin of this modulation has been attributed

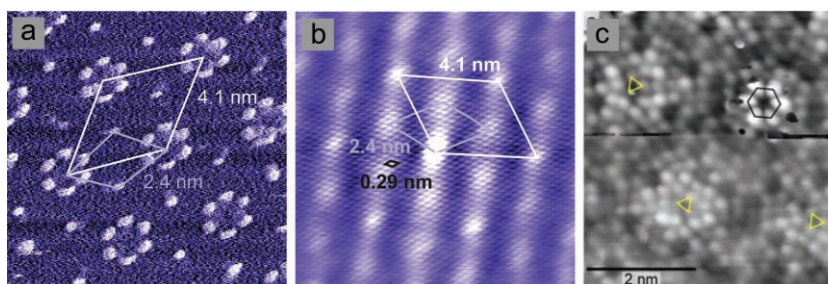


Figure 8. The ultrathin Al₂O₃ film on the Ni₃Al(111) surface. a) An FM nc-AFM damping image, which represents the unit cells of the two superstructures. b) Self-correlation taken from an atomically resolved image (see Ref. [188]). It represents the geometric relation between the two superstructures. c) STM image with atomic resolution at the two different surface sites that form the two superstructures. Panel (c) reproduced with permission.^[191] Copyright 2006, American Physical Society.

to a pinning of the oxide film lattice on a supermesh, which is in coincidence with the atomic lattice of the Ni_3Al substrate.^[188] Quite recently, it has been shown that STM achieves atomic resolution on the film. STM images show that the nodes of the 4.1 nm lattice correspond to holes in the film.^[191] Although this interpretation is supported by DFT calculations,^[191] it has not yet been proven that the proposed film structure is the most stable one.

The examples of alumina films demonstrate yet again how collaboration between STM and nc-AFM aids the understanding of surface structure by providing different, but complementary, information. For the $\text{Al}_2\text{O}_3/\text{Ni}_3\text{Al}$ (111) film, a combination of STM and nc-AFM in a QPlus sensor setup^[5,56] could be used in the future to finally resolve the true atomic structure. The combination of STM and nc-AFM provides a full set of images (topography, current, detuning, and damping) containing different types of tip–surface interactions to aid the atomic-structure analysis of the film. This combination is not restricted to alumina films, but can certainly be used for wider variety of thin insulating films on metal and semiconductor substrates, opening new avenues in the atomic-structure analysis of thin-films.

2.7. Imaging Metallic Nanoclusters

Interest in studying metallic nanoparticles has increased rapidly in the last decade, particularly due to the discovery of their surprising chemical activity when adsorbed on insulating substrates.^[143,144,167,192] These nanocatalysts remain a topic of intense research, with many questions over the mechanisms of their reactivity still open. Since the insulating nature of many of the relevant substrates prevented the use of STM in most cases, AFM has become a common tool for local characterization of these systems.

Almost as soon as the technique became available, nc-AFM was also applied in studies of adsorbed nanoclusters: Au on alumina,^[193] TiO_2 ,^[194] NaCl ,^[195] KBr ,^[196–201] RbI ,^[198] mica,^[202]

MoS_2 ,^[229] poly-L-lysine coated mica,^[203] Si ,^[204] InSb ,^[205] graphite^[206] and gold,^[206] Ag on graphite^[207] and quartz,^[208] Cu on alumina,^[209,210] Pd on alumina^[209,211] and $\text{MgO}(001)$,^[212] Ni on alumina,^[213] Fe on NaCl ,^[214] Fe/Pt on NaCl ,^[214,215] InAs on GaAs,^[202] Si on CaF_2 (111),^[216] and Ge on Si .^[217,218] In terms of resolution, many of these studies offered little benefit over contact AFM measurements,^[219–224] but the extra sensitivity improved the reproducibility of the measurements and reduced unintentional surface damage. Nanoclusters have been successfully manipulated with nc-AFM,^[202–204,225] but manipulation in the dynamic modes of AFM remains difficult and prone to oscillation instabilities due to the large forces involved.

One of the main aims of nc-AFM studies of nanoclusters on surfaces is to provide high resolution of both the cluster and the surface and ultimately to offer atomic scale details about sizes, shapes, and adsorption sites of the clusters. Efforts in this direction have generally focused on the relatively easy to prepare model systems, such as Au nanoclusters on alkali halide surfaces.^[37,196,197,200,201,226,227] These studies often provided atomic resolution on the insulating substrate.^[196,200] However, at close approach nanoclusters are imaged only as fuzzy hemispheres,^[196,200] hiding their true geometric shape^[143] (Figure 9). This is mainly due to the convolution of the tip with the nanocluster.^[196,228,229] For small, nanometer-sized clusters the tip apex is effectively much larger and the shape of the tip apex is what is mostly imaged.^[196] Significant improvements in the resolution of nanoclusters can be achieved by imaging in the constant height mode,^[37] where the tip convolution effect is greatly reduced (Figure 9b–d). An extensive experimental and theoretical study of Pd nanoclusters on MgO (001) showed that the real shape of the clusters could be seen in constant height mode, independent of the shape of the tip.^[38] None of these studies have demonstrated real atomic resolution of a nanocluster, although careful approach to a nanocluster pinned at a step-edge has revealed some internal structure.^[196]

Future studies will certainly push the resolution limits but, perhaps more importantly, an early success combining nanocluster and molecular deposition^[199] suggests that experiments

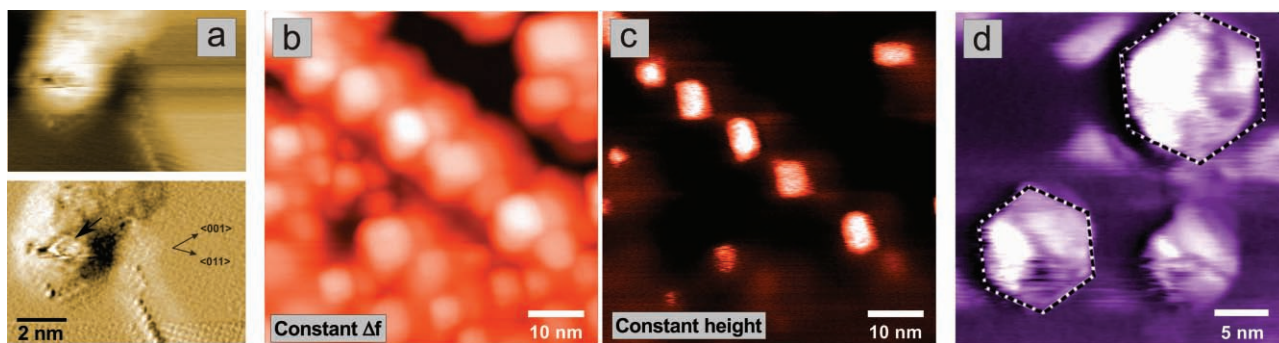


Figure 9. Imaging clusters with the nc-AFM. a) A gold cluster on KBr (001) imaged in the topography mode. Top: topography image, bottom: the corresponding image showing contrast in Δf . The cluster has a size of a few nanometers, comparable to the tip radius, so that the tip, rather than the cluster (fuzzy object), is imaged. Only if the tip is close to the cluster, can a few details of the top facet of the cluster be imaged. Constant- Δf topography image (b) and constant-height image (c) of the same palladium clusters on MgO (001). The tip–surface convolution, which appears in the topography image, is greatly reduced if the clusters are scanned in the constant-height mode. d) A constant-height image of copper clusters on bulk $\alpha\text{-Al}_2\text{O}_3$ (0001) exemplifying the improvement in resolution. Panel (a) reproduced with permission.^[196] Copyright 2004, Institute of Physics. Panels (b,c) reproduced with permission.^[38] Copyright 2008, American Institute of Physics. Panel (d) reproduced with permission.^[210] Copyright 2008, American Chemical Society.

will soon be able to look at products of molecular reactions on nanoclusters in atomic detail. Combined with the ability to look at charge transfer and polarization via KPFM^[195] (see Section 3) and the use of STM for nanoclusters on thin insulating films,^[230] SPM offers a very powerful toolbox for studying these key systems.

2.8. Adsorbed Molecules and Atoms

The adsorption of atoms and molecules on insulating surfaces is central to understanding catalysis, designing molecular electronics devices, and studying molecular magnetism. Through imaging topography, scanning probes can determine adsorption sites and the geometry of an adsorbed species and hence provide the understanding of their binding to a surface. Temperature-controlled measurements can give information regarding diffusion rates of adsorbates and their interaction with surface defects. Tip-induced manipulation can produce new structures and initiate chemical reactions. All these properties have been studied on individual atoms and molecules at conducting surfaces using STM.^[231] However, successful application of nc-AFM in this area came much later. Since individual formate ions on the TiO₂ (110) surface have been imaged using FM nc-AFM some 15 years ago^[153] and the combined STM/AFM studies of porphyrins on copper,^[233,234] high-resolution studies on individual well-separated atoms and molecules are still rare. Theoretical calculations and experimental measurements^[163,232,235] indicate that the tip-sample separation is usually significantly smaller during atomic-resolution imaging with nc-AFM rather than with STM. Hence, the interaction of the tip with weakly adsorbed atoms or molecules can change their position and configuration or cause the adsorbate to be removed by the tip.^[98] This makes atomically resolved nc-AFM imaging of individual species, as well as their controlled manipulation at surfaces, technically very challenging.

Determining the chemical adsorption site of a molecule usually requires simultaneously resolving both the adsorbed molecule and the atomic structure of the substrate. This is a challenge for both STM and AFM studies and requires the preparation of stable and sharp tips. Polar or metallic tips facilitate atomic resolution on ionic surfaces,^[9] but such tips can also interact strongly with an adsorbed molecule and thus prevent stable imaging. To obtain reproducible, high-resolution imaging of both a surface and an adsorbed molecule, the tip should interact strongly with the surface atoms but not with the adsorbed molecule. Further, to determine an adsorption site from an experimental image, one needs to chemically identify the positions of individual surface atoms. Here, one possible strategy is to first identify the ions or atoms of the surface in atomically resolved images, e.g., whether a bright spot in an image is a surface Na⁺ or Cl⁻ on NaCl (001), and then identify the adsorption site. This can be done by experimental observations (see Section 2.4) and/or theoretical modeling of the tip-surface interaction (see Section 2.2). An alternative approach is to solve the inverse problem: one can use a theoretically predicted adsorption site of an adsorbant (e.g., molecule or metal atom) and the image to chemically identify surface ions or atoms.

An example of the first approach is the determination of the adsorption sites of Au atoms on the alumina film grown on NiAl (110).^[185] The measurements were performed using a combined nc-AFM/STM and metallic tip at 5 K. In this case the low symmetry of the alumina film helped to determine that Au atoms preferentially bind to surface Al atoms located above an Al atom of the NiAl substrate. Earlier studies used a combination of nc-AFM and KPFM to establish three different adsorption sites of Pt atoms on the TiO₂ (110)-(1x1) surface.^[236] More recent studies used the earlier understanding of the contrast patterns of the substrate to establish the adsorption sites and configurations of cytosine on the CaF₂ (111) surface,^[237] and perylene derivatives^[238] (Figure 10a) and terephthalic acid^[239] on the TiO₂ (110) surface.

The second approach has been used in nc-AFM studies of individual molecules of Co-Salen (Figure 10b), a small chiral paramagnetic metal-organic Schiff base complex, on the NaCl (001) surface using Cr-coated tips at 30 K.^[240,241] The obtained images simultaneously exhibit both the position and the orientation of the adsorbed molecules and the atomic structure of the surface, enabling the determination of the exact adsorption site. Density functional theory calculations were used to identify the ionic sublattice resolved with the Cr tip and also to confirm the adsorption site and orientation of the molecule on the surface. Imaging molecules at room temperature is more challenging. Custom-designed syn-5,10,15-tris(4-cyanophenylmethyl) truxene molecules were imaged with atomic and molecular resolution at room temperature using nc-AFM at the nanoscale structured KBr (001) surface.^[242] The molecules were observed rapidly diffusing along the perfect monolayer step edges and immobilized at monolayer kink sites. Extensive atomistic simulations elucidate the mechanisms of adsorption and diffusion of the molecule on the different surface features. The results of this study suggest methods of controlling the diffusion of adsorbates on insulating and nanostructured surfaces.

A different approach has been used to image pentacene with atomic resolution using nc-AFM/STM on patches of ultrathin NaCl layers deposited on Cu (111) at 5 K.^[64] In this system, tunnelling is still possible and suitable tips could be prepared on the bare metallic substrate in the STM mode using standard procedures to transfer certain atomic or molecular species from the surface to the tip apex.^[243] Such well-controlled procedures currently do not exist for pure nc-AFM measurements, particularly not on bulk insulating surfaces. A tip functionalized with a CO molecule in this manner was then used in the nc-AFM mode to image pentacene molecules adsorbed on the NaCl islands with submolecular resolution (Figure 10c-h). Modeling played a vital role in determining the mechanism of submolecular resolution resulting from the interaction of the CO-terminated tip and pentacene, with the authors concluding that Pauli repulsion is the main source of atomic contrast in the molecular image. This approach has been later used to provide a detailed chemical model for a previously misassigned molecule, cephalandole A.^[244] Similarly, nc-AFM investigations of adsorbed molecules on mica and TiO₂ surfaces^[245,246] combined with theoretical modeling suggest that the repulsive regime of contrast formation can be identified and controlled by analyzing origins of contrast inversion in images. This goes beyond the common perception that the best and most non-invasive

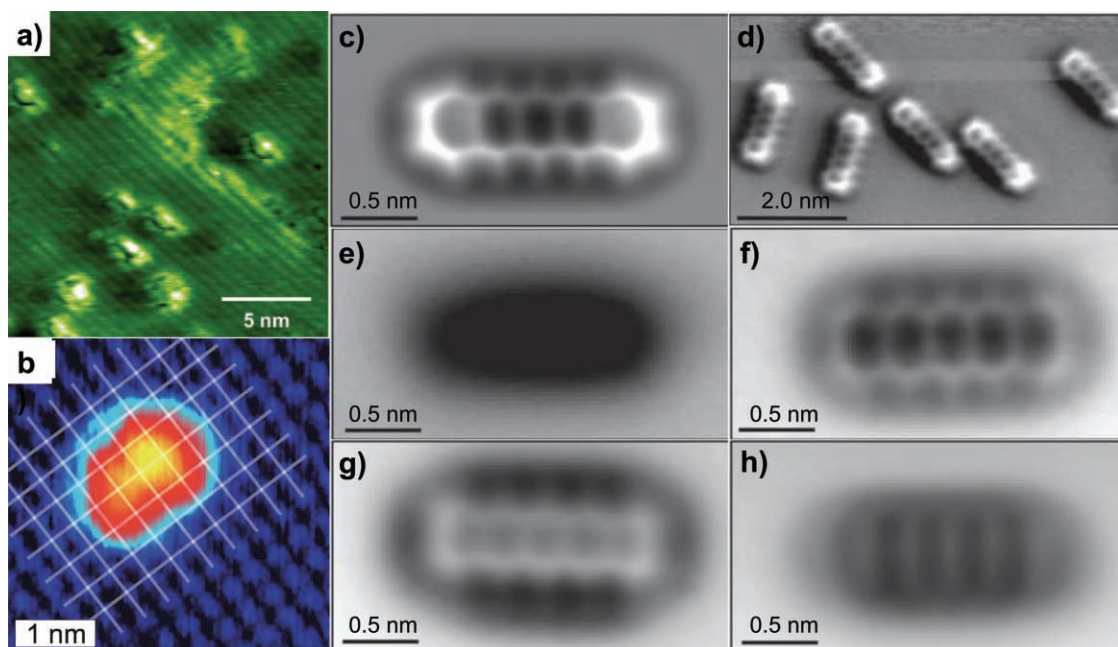


Figure 10. nc-AFM images of a) perylene adsorbed on TiO_2 (110), b) Co-salen adsorbed on NaCl and pentacene adsorbed on thin NaCl films on copper using different tip terminations. c,d) CO molecule, e) Ag, f) CO, g) Cl, and h) pentacene. Panel (a) reproduced with permission.^[237] Copyright 2009, American Physical Society. Panel (b) reproduced with permission.^[240] Copyright 2009, Institute of Physics. Panels (c–h) reproduced with permission.^[64] Copyright 2009, American Association for the Advancement of Science.

contrast can be achieved in the attractive regime of tip–surface interaction.

Controlled manipulation of atoms and molecules with nc-AFM tips is now becoming a reality.^[10, 33] Significant success has been achieved at semiconductor surfaces since the earliest publications.^[247–249] Despite several theoretical studies

suggesting that manipulating atoms at insulating surfaces should be feasible,^[250–252] experimental breakthroughs proved much more difficult to achieve. Tip-induced displacements of atom-sized defects on a CaF_2 (111) surface at room temperature have been observed^[98] and similar results have been obtained on the KCl (100) surface.^[253] In these studies, the defects were dragged by the nc-AFM tip along the slow-scan direction at given threshold tip–surface distances. However, achieving controlled manipulation still requires achieving much better control over the tip structure and the balance of forces between the tip, the surface, and the manipulated species.

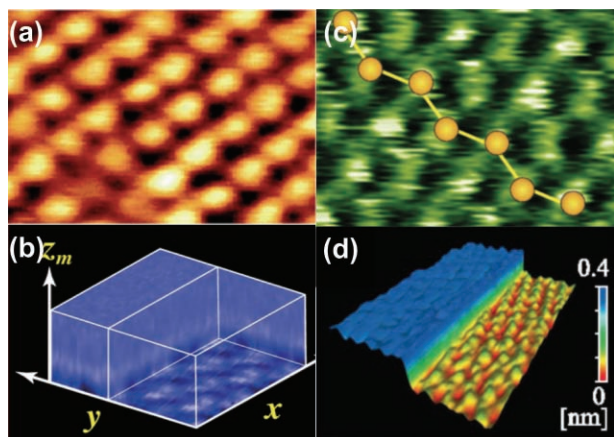


Figure 11. Examples of atomically resolved nc-AFM experimental images in liquid. a) 2D and b) 3D images of the mica surface in water. c) Calcite (10-14) surface in water. d) Dipalmitoylphosphatidylcholine (DPPC) lipid bilayer in a phosphate buffer saline (PBS) solution. Panel (a) adapted with permission.^[272] Copyright 2010, American Physical Society. Panel (b) adapted with permission.^[86] Copyright 2010, American Physical Society. Panel (c) adapted with permission.^[273] Copyright 2009, American Chemical Society. Panel (d) adapted with permission.^[274] Copyright 2007, American Physical Society.

2.9. Imaging in Air and Liquids

Although many of the recent success stories of AFM have been achieved in UHV conditions, for most applications this is not a particularly relevant environment, e.g., studies in air or ambient gases would be more relevant for catalysis^[143] and studies in liquid would mimic the physiological conditions relevant to biological systems.^[48] Furthermore, controlling the environment offers the possibility of damping van der Waals interactions and removing capillary forces.^[254] Of course, the first AFM studies were in air^[255,256] and some early high-resolution studies were in water.^[41] In these studies, AFM is operated in contact mode and suffers from similar problems to studies of systems in UHV in contact, i.e., the imaging process is invasive and the large lateral tip–surface forces damage or deform the sample. Recent contact studies have improved on this,^[257] but it is particularly a problem in organic or biological systems, where molecules are often only physisorbed to the surface by

weak van der Waals interactions. Imaging these systems is possible if the molecules are firmly attached to the surface or form a crystal structure,^[69,258–263] but even for high-resolution studies on predominantly flat surfaces,^[41] in contact mode it is very difficult to understand whether AFM really sees the surface or just a convolution of surface, tip, and liquid molecules.

A natural route to reduce the lateral forces experienced by the sample is to reduce the amount of time the tip spends in contact by introducing vertical cantilever motion.^[34] Instead of contacting the surface throughout the scan, the tip only contacts the surface gently at the closest approach of the oscillating cantilever. A mode of AFM operation using amplitude modulation (AM) (see Section 2.1) is known as tapping mode or intermittent contact.^[264] It has proven very successful for imaging samples in liquid,^[7,265–267] and its capability for high-resolution studies in physiological conditions has led to AFM becoming the tool of choice for the investigation of biological systems.^[48,268] However, its ultimate resolution is limited to the nanometer level by the low quality factor of the cantilever resonance in air and liquid environments causing high noise.^[34,269] The same problem prevents conventional FM-AFM in air and liquids from offering comparable resolution to that commonly seen in UHV. For a standard microfabricated silicon cantilever, the Q factor is 10 000–200 000 in vacuum, 300–600 in air, and 1–20 in liquid; molecular resolution is estimated to be possible down to Q values of around a few hundred.^[270] Despite reduced viscosity, imaging in inert gases offers similar quality to imaging in air, with a Q value of about 500 using conventional amplitudes.^[271]

It was recognized fairly early in the development of FM-AFM that stiffer cantilevers and small amplitudes could offer dramatic increases in the signal-to-noise ratio and Q .^[49] Generally, low-amplitude, stiff cantilevers are fabricated from quartz tuning forks and appropriate tips are glued to the end of a beam,^[55,56,275] but stiff metal cantilevers have also been used.^[276] Despite increased difficulty in preparation, low-amplitude studies have been very successful in UHV atomic-resolution studies of several insulating surfaces and thin films,^[61,102,178,277,278] and have also been used to study water nanoclusters on mica in air.^[279] Even conventional silicon cantilevers can be operated at low amplitude and this has proved to be a breakthrough in high-resolution imaging in liquids.^[270,273,280,281] Using ultrasmall amplitudes of tenths of a nanometer, the low Q outside UHV is compensated and lateral resolution of a few hundred picometers was achieved in water on molecular crystals,^[280,281] mica,^[272] and a lipid bilayer (see Figure 11).^[274] Refinements in sensitivity offer the potential for an order of magnitude improvement in resolution^[282] and the use of small cantilevers could improve this further. Recent developments in speed and control mean it is possible to perform 3D imaging in water, and this was applied to obtain unprecedented resolution of the structure of water layers on mica.^[86] Beyond FM-AFM, phase modulation can significantly improve the imaging speed in liquids^[283] and oscillating the cantilever laterally in torsional resonance mode^[284,285]

again increases sensitivity and has been successfully applied to studies in liquids.^[286] Most recently, small-amplitude AM-AFM has demonstrated high resolution of a wide variety of substrates in liquid conditions.^[287]

In the future, molecular and atomic resolution in air and liquids is certain to become almost routine and greater efforts will be made in interpretation and understanding the influence of the environment on both the measurement and the sample. In this direction, combining SPM techniques will again be a powerful approach, with the capabilities of the electrostatic mapping that KPFM would offer in characterizing biomolecules in physiological conditions being particularly promising.

3. Long-Range Electrostatic Forces in AFM

As discussed above, one can rarely determine the chemical nature of surface atoms or supported nano-objects from imaging the surface topography alone. In most cases, a combination of experiment and theory (see Section 2.2), doping crystals with known impurities (see Section 2.4), or decorating surface sites with known adsorbates (see Section 2.8) are needed to achieve unambiguous chemical identification. It has long been realized that measuring the long-range electrostatic forces may assist chemical identification. As illustrated in Figure 12, nano-objects of different chemical composition (metal or insulating films, ions, molecules, etc.) change the local electrostatic surface potential by changing the local work function of a metal surface.^[288–292] Such nano-objects also change the local electrostatic potential when supported on an insulating surface. Measuring the local work function or electrostatic potential of a surface by AFM with a resolution in the mV range and at the nanometer scale could be used for chemical identification of surface species. Apart from other electrostatic AFMs like electrostatic force microscopy (see Table 1 and references therein), this can be achieved using KPFM, which has become a well-established surface science tool in many scientific disciplines.^[23,24,293]

KPFM is a very effective technique for directly measuring the contact potential difference between the conducting tip and conducting surface.^[21,22] In such a measurement, a direct current (dc) (U_{dc}) and an alternating current (ac) voltage (U_{ac}) with frequency f_{ac} are applied between the tip and surface. Owing to

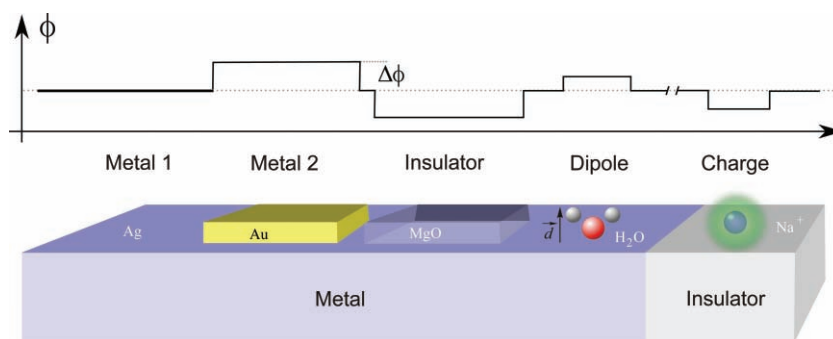


Figure 12. Objects of different chemical compositions exhibit differences in the local work function on the surface (metal) or in the electrostatic surface potential (insulators), which can be used for the chemical identification in AFM.

the modulation of the electrostatic force by the ac voltage, the electrostatic contribution, oscillating at frequency f_{ac} and also at $2f_{ac}$, can be extracted (first and second harmonic). The first harmonic includes a term with $U_{dc} + U_{CPD}$, in which U_{CPD} is the contact potential difference between tip and surface. By varying the dc voltage such that the first harmonic becomes zero ($U_{dc} = -U_{CPD}$), the total electrostatic tip–surface interaction is minimized at each point on the surface. The contact potential difference between the tip and surface is then given by $U_{dc} = -U_{CPD} = (\varphi_{sample} - \varphi_{tip})/e$ where φ_{sample} and φ_{tip} are the work functions of the sample and tip, respectively and e is the electron charge. At two different locations on the surface (positions 1 and 2), the difference ($U_{dc, pos1} - U_{dc, pos2}$) $e = (\varphi_{pos1} - \varphi_{tip}) - (\varphi_{pos2} - \varphi_{tip}) = \varphi_{pos1} - \varphi_{pos2} = \Delta\varphi$ yields the work function difference between these locations.

In most cases the Kelvin modulation technique is applied during normal nc-AFM topography imaging. Depending on the ac frequency, one distinguishes between frequency-^[294] and amplitude-modulated^[295] KPFM (see also Refs. [296,297]). An independent feedback loop regulates the dc voltage so that $U_{dc} = -U_{CPD}$ is achieved at each point on the surface. Both topography and a so-called Kelvin image of $U_{dc} = -U_{CPD}$ are obtained at the same time in one measurement, where the Kelvin contrast corresponds to local variations of the surface work function. If insulating surfaces are imaged, fixed charges or dipoles, which change the local electrostatic surface potential, determine the contrast in the Kelvin image.^[298–300] In the literature many different aspects of the Kelvin technique can be found.^[21–23,294–297,301–303] Below we present several examples of recent KPFM applications, which deal with metal–insulator interfaces and defects at insulating surfaces.

3.1. Thin Insulating Films on Conducting Surfaces

A convenient way to study insulating surfaces is to prepare a thin insulating film on a conducting support. On such films, charging experiments can be performed, where charges can be created by different methods with the tip: contacting the tip with the surface, by corona discharge from the tip, or by inducing tunneling of electrons from the conducting support into the thin-film or vice versa. Most experiments of this type were done in air by EFS and EFM on SiO_2 ,^[304] Si_2N_3 ,^[305] Al_2O_3 ,^[306,307] GaN ,^[308] and PMMA ^[309] films and also on nano-

clusters embedded into or supported by thin SiO_2 films.^[310–313] In UHV, such experiments can be more precise, such that single electron processes can be studied.^[299,314]

An important application of KPFM is to measure work function changes of conducting supports induced by adsorbed thin insulating films, which can be best realized under the clean conditions of UHV. In most cases, thin insulating films are prepared in such a way that they only partially cover a conducting surface, so that the work function difference between the conducting support and the film can be directly imaged by the Kelvin microscope (Figure 13). Spectroscopic measurements^[315–317] and theoretical calculations^[289,290,292,318] demonstrate that NaCl, KBr, or MgO thin-films lower the work function of metal substrates. This work function change has been quantitatively measured at the nanoscale by KPFM for LiCl, NaCl, KCl, and RbCl films on Au (111);^[319] for NaCl and KBr films on Cu (111);^[320] for KBr films on Ag (111);^[321] and for MgO thin-films on Ag (001).^[180,324] The lowering of the surface work function has also been found on semiconductor substrates, e.g., in the case of KBr (001) thin-films on InSb (001).^[322,323]

A very important issue is whether KPFM on thin insulating films can achieve high lateral resolution and accurately measure a work function difference between a film and a conducting support. Although a change in the surface work function at a film–support boundary can be observed with nanometer resolution,^[320] the work function plateaus only at very large distances from the boundary. In fact, in most cases work function differences are correctly measured at distances of 50–100 nm from the boundary.^[297,319,320,323] As the electrostatic tip–surface interaction is of long-range character, the size of the whole tip apex is then responsible for the accuracy of the work function measurements. The importance of this effect has been clearly demonstrated on one-layer-thick MgO (001) islands grown on Ag (001); the effective radius of the tip apex is often larger than the 5–10-nm-large islands and the work function difference has much smaller values than expected.^[324] However, tip changes occur quite frequently in such experiments, which leads occasionally to a sharp, neutral nanotip at the apex and, in turn, to a better representation of true work function differences.^[180]

Insulating thin-films are also important buffer layers in molecular electronics, where molecules are electronically decoupled from the conducting support by the thin-film. Since the coupling between the conducting support and the

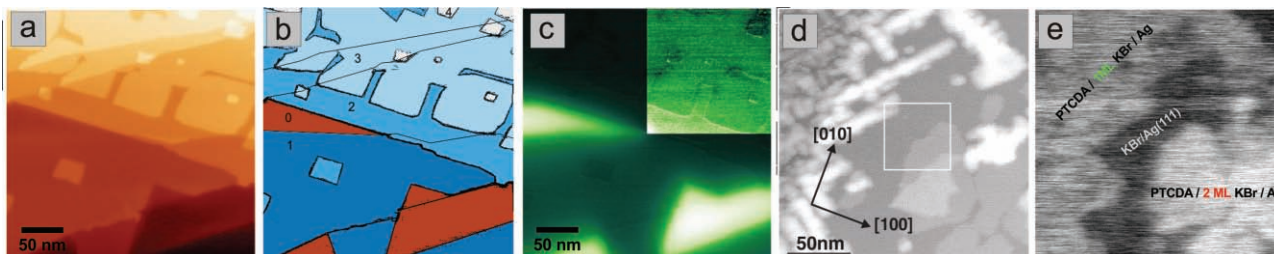


Figure 13. KPFM on thin-films. a–c) NaCl films on Cu (111) (topography (a) and corresponding Kelvin image (c)). The drawing in panel (b) shows the different layers of NaCl (0: Cu, 1–3: 1–3 ML NaCl). d,e) Perylene-3,4,9,10-tetracarboxylic-3,4,9,10-dianhydride (PTCDA) on 1 and 2 monolayer (ML) KBr on Ag (111). If PTCDA is located on 1ML KBr, clusters and rods are formed (topography image (d)). On 2ML KBr, a closed regular film is formed. Both types of molecular films exhibit large differences in the work function of the Ag (111) surface (see Kelvin image e). Panels (a–c) reproduced with permission.^[320] Copyright 2009, Institute of Physics. Panels (d,e) reproduced with permission.^[321] Copyright 2006, Institute of Physics.

molecules varies with the thickness of the insulating film, the electronic properties, such as the work function, of such heterostructures can be tailored. This effect has been quantitatively imaged using KPFM for PTCDA and Alq₃ molecules adsorbed on the KBr (001)/Au (111) surface.^[321,325] These measurements exhibit clear differences in the surface work function if molecules are supported either on the gold surface or on one- or two-monolayer-thick KBr (001) islands (Figure 13d,e).

The recent progress in nc-AFM using functionalized tips and a combination of STM and nc-AFM on molecules supported on thin-films shows that each atom of a molecule can be imaged.^[64] Besides the atomic structure, the electronic properties of a molecule are also important. By scanning tunneling spectroscopy, the electronic states close to the Fermi level can be probed.^[326,327] On the other hand, inelastic tunneling spectroscopy is able to measure vibrational properties of the molecule.^[326,327] Here, KPFM measurements could provide additional information on the local surface work function at the molecule and on the presence of extra charges or dipoles inside the molecule.

In the case of metal nanoclusters on ultrathin films, KPFM could be used to image directly charge transfer between the conducting support and nanoclusters, which has been predicted by theory^[290,292,318,328] and experimentally observed by spectroscopy methods and STM on MgO thin films.^[318,381] Furthermore, the tip can be used to intentionally charge single nanoclusters and to afterwards observe the charge evolution from the cluster into the support as a function of time, which is important for applications in nanotechnology and surface chemistry.

3.2. Individual Defects on Bulk Insulating Surfaces

Defects of atomic size, such as vacancies, play an important role in the chemistry of insulating surfaces. As most of these defects are chemically active, their characterization can only be done in UHV. One can attempt to identify defects by combining nc-AFM and KPFM as follows: the surface and defects are first imaged with high- or even atomic-resolution by nc-AFM, then Kelvin microscopy is performed at the same position on the surface. Images with atomic resolution supply information on the atomic structure of the surface, whereas the Kelvin images yield information about the charge state (sign and strength) of the surface defects. With this, and the knowledge of the material's properties, it is possible to determine the electronic state and, under specific circumstances, the chemical nature of the considered defects.

Defect identification by KPFM has first been demonstrated on semiconductor surfaces. For instance, topography images of the UHV-cleaved p-WSe₂ (0001) surface exhibit a very faint contrast of small defects on the terraces, whereas corresponding Kelvin images show a bright or dark Kelvin contrast at these places.^[329] Due to the Kelvin contrast, such defects can be identified as negative (bright) and positive (dark) dopants, which would not be possible to conclude from the topography images alone. Similar observations have been made on p- and n-type doped SiO₂ films on Si (111),^[330] on UHV cleaved n- and p-type doped GaAs (110), and on p-type doped GaP (110) surfaces.^[331]

On the latter surfaces, large differences in the Kelvin contrast at steps have been observed and assigned to a downward and upward band bending due to localized charged dopants.

Recently, it has been shown that KPFM can also yield valuable information for the identification of defects at surfaces of bulk insulators, such as the (001) surfaces of bulk alkali-halide crystals. An important question is what KPFM is actually measuring on an insulating surface. In KPFM, an external potential is applied between the tip and the metallic sample holder and the electrostatic field penetrates the insulator. The Kelvin microscope measures then the contact potential difference between the tip and the sample holder, which is modified by the insulator between the tip and sample holder.^[20] The valence and conduction bands of the insulator are usually positioned such that the Fermi level of the metallic sample holder is in the band gap of the insulator.^[332] However, because the (001) surfaces of alkali-halide or MgO crystals are mostly prepared by in situ cleavage,^[50] a significant region below the new surface is damaged due to the large uncontrolled stress that is applied during the cleavage. This produces defects in the bulk and especially at the surface, many of which are charged. As a result, the sample is charged, strongly influencing the Kelvin voltage,^[18] and shifts of tens of volts have been measured by KPFM.^[50,52,333]

Surface charging after cleavage hampers imaging with high resolution.^[50,52,333] To avoid this, in situ cleaved alkali-halide or MgO crystals are usually annealed at high temperatures prior to AFM experiments to remove most of the charge. After achieving an equilibrium charge state by annealing, a faint contrast at the defects is observed in KPFM images due to residual charges on the surface.^[52] In the case of alkali-halide surfaces, bright patches at steps correspond to a more negative surface potential in comparison to the neutral and stoichiometric terraces. At each patch, nc-AFM imaging with atomic resolution reveals single atomic-sized defects, which are located at kinks and corners of steps^[300] (Figure 14). In fact, such measurements are in perfect agreement with the model of the surface double layer (Debye-Frenkel layer),^[334,335] where alkali-halide surfaces have a negative net surface charge at room temperature.^[336–339] The negative charge is due to the negative cation vacancies at kinks and corners,^[340] which locally change the electrostatic surface potential. A similar mechanism can be found at dislocations, which are also reservoirs of positive or negative defects.^[335] Recent KPFM and atomic-resolution imaging on KBr (001) have proven the existence of charged vacancies at dislocations and an identification of the defects could be made^[341] (Figure 15).

A net negative surface charge was also observed at Suzuki precipitates on Cd²⁺- and Mg²⁺-doped NaCl crystal surfaces,^[134,135] resulting from the negative cation vacancies inside the Suzuki structure. On MgO (001), the net surface charge was found to be negative,^[212] contrary to the expected presence of positive F⁺ or F²⁺ centers on the MgO (001) surface.^[342,343] Despite an occasional dark Kelvin contrast at some places on the surface due to the possible presence of F centers, it was concluded that most of the F centers have probably reacted with the residual gas in the UHV, forming negative species such as charged O₂⁻ or CO⁻ radicals at low coordinated surface sites.^[328]

These few examples show that KPFM helps in identifying charged surface defects, which is not possible from nc-AFM

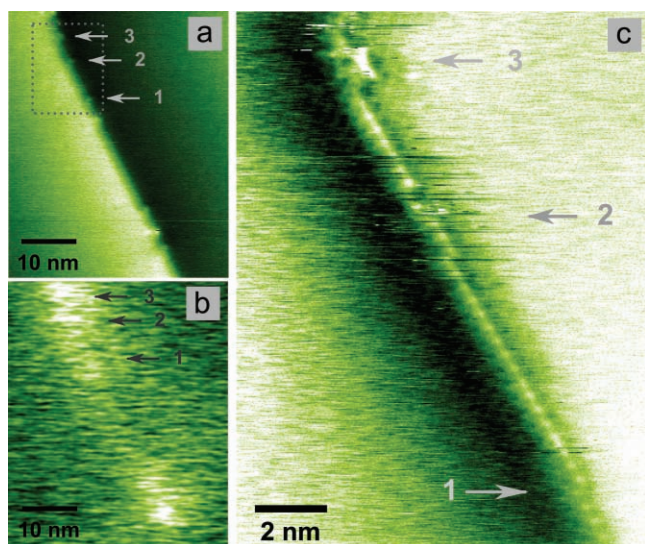


Figure 14. The surface double layer (Debye-Frenkel layer) on ionic crystal surfaces. The topography image (a) shows a step, at which bright patches can be seen in the Kelvin image (b). Atomic-resolution imaging in the constant height mode (c) reveals a kink at each bright patch (compare positions 1–3). The bright patches in the Kelvin image are a result of negative cation vacancies, which are located at the kinks and which produce a more negative surface potential with respect to the perfect and neutral terraces. The images were recorded on the NaCl (001) surface. Reproduced with permission.^[300] Copyright 2006, American Chemical Society.

topography images alone. The sensitivity of KPFM is sufficiently high to detect charges with an equivalent amount of less than one electron.^[298,300,344] This provides the possibility to use a combination of nc-AFM and KPFM also on other surfaces. Candidates for the future are ionic crystal surfaces like the (111) surfaces of fluorites, oxide surfaces, and even more complex surfaces. A challenge is to apply nc-AFM and KPFM on surfaces where atomic resolution has not yet been well understood. For instance, the (111) surface of CeO₂ exhibits a variety of point defects, which still urgently need identification.^[103]

A further important challenge is achieving atomic resolution in KPFM. A few examples already exist where atomic resolution could be obtained, and reasonable understanding has been achieved for ideal ionic^[345–347] and more complex surfaces.^[348,349] Moving beyond this to understanding high-resolution images of defects, thin films, molecules, and clusters still requires significant efforts. However, these efforts are strongly motivated by the demonstrated potential of KPFM to capture electrostatic changes due to localized charging and chemical reactions in a wide variety of systems.^[350,351]

3.3. Metal Nanoclusters on Insulating Surfaces

Another major challenge of KPFM is characterizing supported nano-objects, such as metal clusters. Metal nanoclusters on insulating oxide surfaces play a particularly important role in catalysis by promoting many chemical reactions;^[143,144] a marked

example is the oxidation of CO on Au/TiO₂.^[352] Recently it has been realized that a support can change the electronic and, therefore, the catalytic properties of the clusters.^[144] This has been shown to be crucial, for example, in the case of ultrathin MgO (001) films,^[289–291,353,354,381] where supported gold clusters become charged by the metal support beneath the insulating film. Since charge transfer modifies the electronic structure and related properties, such as the work function of large clusters, KPFM is a promising technique for studying charging of individual clusters with nanometer resolution. In the following, large clusters are defined as those containing at least 1000 atoms. For such clusters the ionization potential equals the work function of the bulk material.^[355]

Simple surfaces demonstrating KPFM works quite efficiently are conducting surface systems (e.g., metal clusters or films on metal surfaces), which have been studied in air^[312,356–359] and also in UHV.^[205,294,296] KPFM can accurately probe work function differences between large clusters and a substrate surface with a lateral resolution at the nanometer scale and with the energy sensitivity in the mV range. This has been tested by growing gold clusters on graphite.^[296] or on silicon.^[294] Such work function measurements can even reveal an alloying between the substrate and the clusters, as has been observed on Au/InSb(001)^[205]

On the surfaces of bulk insulators, KPFM has been mainly used to study metal clusters on alkali halide and MgO crystal surfaces. In such experiments, the bulk insulator separates the clusters from a conducting support (metallic sample holder), so that no conducting channels exist between the clusters and the support. This aspect is important especially when charge is transferred between a cluster and the tip during contact. The charge stays for a very long time on the cluster and electrons can be transferred only to the neighboring clusters located at nanometer-scale distances from the charged cluster^[195] (Figure 16a,b). When clusters are neutral on the insulating surface, KPFM measures the work function difference between the insulator on the conducting sample holder and large clusters.^[212] However, in most cases, the clusters are influenced by the insulating support, which has been observed for gold clusters on alkali-halide surfaces,^[195] palladium clusters on MgO (001)^[212] (Figure 16c), or even for single platinum atoms on the TiO₂(110) surface.^[236,360]

The resolution in KPFM images of large clusters is greatly enhanced and provides a more accurate measure of the cluster work function in comparison with that of thin insulating films (Figure 16d,e)^[212] This is because the tip is usually several nanometers away from the insulating surface when placed above a cluster (this distance is close to the height of the cluster), so that the electrostatic tip–surface interaction is mainly due to the tip–cluster interaction.

The few existing examples demonstrate that KPFM can indeed image the electronic properties of cluster–surface systems at the nanometer scale. One can thus perform KPFM studies on many other cluster–surface systems, including deposited molecules.^[201] An important challenge is to study very small nanoclusters (e.g., deposited gas-phase clusters), which contain only up to a hundred atoms. Such clusters exhibit strong variations in the ionization potential, which changes drastically if only one atom is added to or removed from the cluster.^[144,355] Differences in the electronic properties

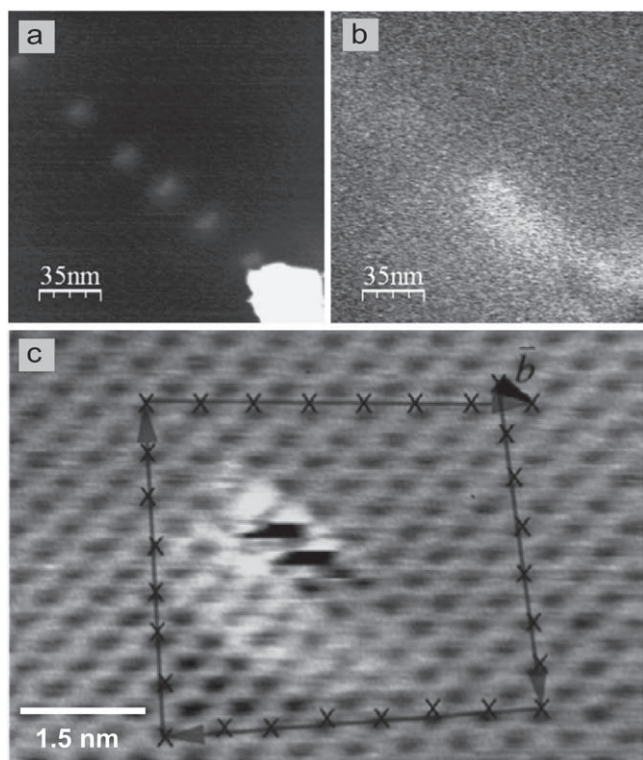


Figure 15. Dislocations on the KBr (001) surface studied by KPFM (a: topography, b: Kelvin image). The topography image (a) shows a string of shallow hillocks emerging from the surface. At the end of one hillock, atomic resolution imaging (c) reveals an edge dislocation, which Burgers vector is represented by the circuit drawn on (c) representing the direction $[1-10]$ and magnitude of the vector $(\sqrt{2}a/2)$. Thanks to the bright Kelvin contrast (b), the defects could be identified as negative defects. Reproduced with permission.^[341] Copyright 1995, American Physical Society.

amongst such small clusters can also be expected if the clusters are supported on a surface, which could be verified by high-resolution KPFM.

As discussed above, a big benefit of AFM in general, is that the tip can be used to explicitly charge metal clusters and then to study the charge state with electrostatic AFMs. The reliability of controlled charging by the AFM tip has been already shown

in EFM experiments,^[310–313] but KPFM should be able to achieve further progress in such experiments due to its much higher lateral resolution and better energy sensitivity. Due to the charge sensitivity of the KPFM down to an equivalent charge of one electron and below^[300,305] and to the capability to inject a single electron into a single atom,^[171] controlled charging experiments of clusters via the AFM tip and characterization by KPFM are within reach.

The biggest promise of KPFM is related to surface chemistry because the classical Kelvin probe already allows one to follow chemical reactions on surfaces by monitoring changes of the surface work function.^[13,14] Preliminary results obtained on Pd/graphite demonstrate that the KPFM is indeed chemically sensitive.^[361] For instance, the contamination of the clusters by constituents of the residual gas at 10^{-10} mbar can be followed on a time scale of some hours (Figure 17, upper panel). Immediately following preparation, the Pd clusters exhibit a bright Kelvin contrast (Figure 17, middle panel), which is due to their higher work function with respect to HOPG. On a timescale of one week, the work function of the Pd clusters drops below the value of HOPG (dark contrast) because of a chemical reaction with the residual gas in the UHV. A high-temperature anneal of the contaminated Pd clusters in oxygen cleans the Pd clusters so that they again exhibit their initial work function (Figure 17, bottom panel). Although the clusters are quite large, size and site effects can be already observed: smaller clusters are more reactive than larger clusters and edges or facets of clusters exhibit a different potential than the top facet of the clusters. These KPFM measurements strongly motivate the use of KPFM as a standard local probe technique for work function measurements of cluster–surface systems of interest in surface chemistry.

4. Outlook

Advances in STM have long allowed insight into the mechanisms and rates of adsorption, diffusion, and reactions on conducting surfaces by directly observing the motions of the individual atoms and molecules involved. However, it is only recently that nc-AFM started catching up with its sister technique in this part of its application spectrum. With rapid

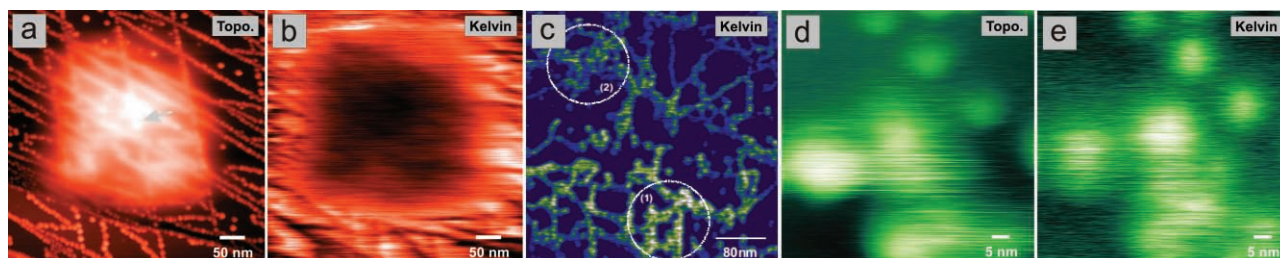


Figure 16. a,b) Gold clusters on NaCl (001) after a contact of the tip with one of the clusters (see arrow in panel (a)). Due to the small cluster–cluster distance of 2.8 nm, charges propagated along cluster rows in an area of 300×300 nm. In both the Kelvin image (b) and the topography image (a) a strong contrast could be observed due to a strong Coulomb interaction with the tip. c) Kelvin image of Pd clusters on MgO (001). The increased contrast at the clusters shows that groups of clusters exhibit different contrast due to different possible charge transfers between the clusters and the substrate. d,e) Similar Pd clusters grown on MgO (001). The lateral resolution is approximately 5 nm. Panels (a–c) reproduced with permission.^[195] Copyright 2006, American Institute of Physics. Panels (d,e) reproduced with permission.^[212] Copyright 2004, Institute of Physics.

Chemical reaction with gas from UHV

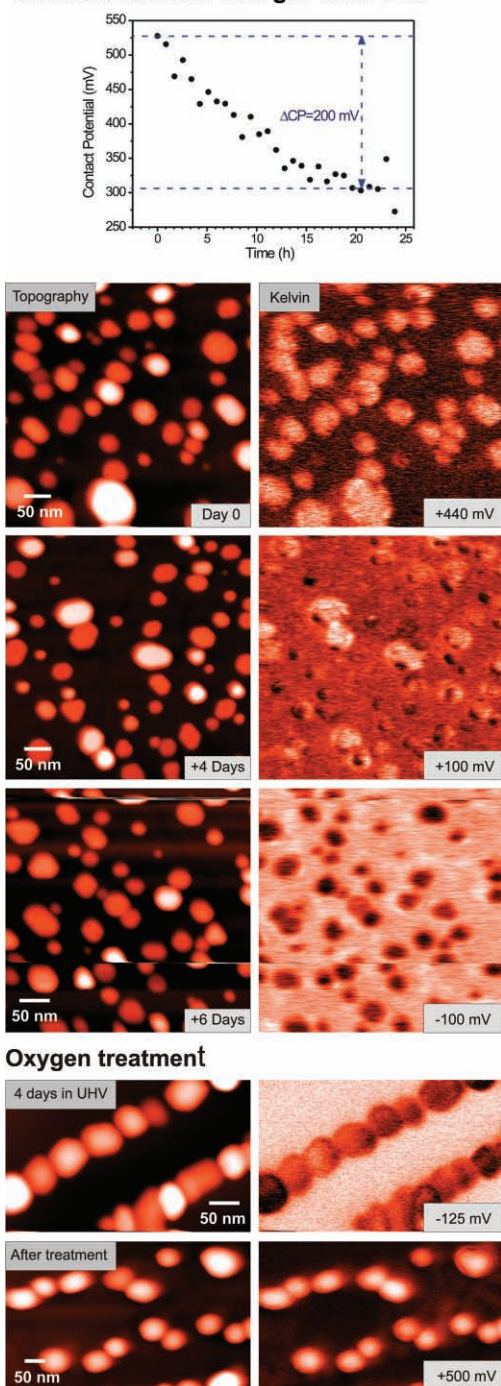


Figure 17. Chemistry of Pd nanoclusters on the HOPG surface. Top: Mean tip–cluster contact potential difference as a function of time. The CPD decreases within hours in a 2×10^{-10} mbar environment due to chemical reactions between the clusters and the residual gas in the UHV. Middle: Each pair of images represents one Kelvin measurement (left: topography, right: Kelvin image). The Pd clusters were left in UHV for 6 days (pressure = 2×10^{-10} mbar). Bottom: Pd clusters left for 4 days in UHV after their preparation and then annealed in an oxygen atmosphere (pressure = 8×10^{-10} mbar) at 500 °C for 30 min. HOPG was prepared by cleavage in air and annealing in UHV at 500 °C for some hours. The Pd clusters were created by evaporation of Pd from a Knudsen cell onto the HOPG surface (3 monolayers of Pd, 400 °C).^[361]

advances in high-resolution imaging in UHV and in solution, nc-AFM is now moving beyond its adolescence and becoming an accomplished and reliable instrument. However, despite the great progress, significant challenges remain. Studies of real chemical processes at surfaces are severely limited because scanning probes are generally slow both in terms of moving from A to B and recording rapid changes in force or current. Using stiff cantilevers with high resonance frequencies, like tuning forks, holds some promise in this area.^[56] Such cantilevers are good candidates for high-speed nc-AFM, as in the case of contact AFM.^[362] Certainly, the constant-height mode will play an important role in this regard, since relatively high scanning speeds of up to 60 Hz can be used already for commercial 300 KHz cantilevers,^[37] opening the door for nc-AFM at video frequencies. More generally, the understanding and interpretation of atomically resolved images is still a major challenge and this limits the uptake of the technique, in spite of the growing sophistication and power of modeling techniques. The problem is of course inherent to all AFM-based techniques because the chemical contrast is directly determined by the chemical composition and structure of the tip apex. Therefore, preparing, controlling, and characterizing tip apices is one of the most pressing issues in high-resolution nc-AFM and is solved only for a few special systems (see Section 2.8). Here again the partnership of nc-AFM with STM and, increasingly, with KPFM helps in understanding the structure and properties of imaged surfaces by complementary deconvolution of the tip from the measured signals.

As we have tried to emphasize, the strength and driving force of AFM is in versatility of different methods and applications. For example, the variation of the work function at individual clusters as a function of adsorbate coverage can be monitored by KPFM. This offers the possibility to measure rates of catalytic reactions at individual nanoclusters. Indeed, for a Langmuir–Hinshelwood mechanism the reaction rate is proportional to the adsorbate coverage. It will then become possible to follow the evolution of the reaction rate and to correlate it with the possible evolution of the cluster shape at a single cluster during a reaction. Also, the development of FM-AFM techniques for high-resolution imaging in solutions (see Section 2.9) are complemented by new methods for studying solid–liquid interfaces in electrolyte environments. In particular, a new design for an electrochemical scanning probe microscope for studies at the solid–liquid interfaces has been recently proposed,^[363] while another design of an electrochemical AFM uses a tip-attached redox mediator.^[364] This latter technique can be particularly suitable for probing the activity of slowly functioning nanometer-sized active sites on surfaces, such as individual enzyme molecules. A trend in optical spectroscopy has emerged that makes use of the interaction of an AFM tip with a sample in an external optical field. Special attention has been devoted to tip-enhanced Raman spectroscopy and to the manipulation of molecules and particles with simultaneous fluorescence. A recent study employing tip-enhanced Raman scattering^[365] showed that the signal-to-noise ratio of the method is good enough to obtain base-specific spectra from a single nucleic acid strand.^[366] These and other similar studies hold great potential for applications such as DNA sequencing, but their application to studying individual chemical species at inorganic surfaces remains in the future.

The application of force microscopies to technological problems is also expanding and often requires the combination of several methods. In particular, scanning capacitance microscopy (SCM) and scanning spreading resistance microscopy (SSRM) are used for implant mapping, whereas conductive AFM (C-AFM) is used for the analysis of thin dielectrics and KPFM is used to study the potential distribution across active electronic devices.^[367] AFM can be also used as a part of nano-optomechanical device, where mechanical changes on the nanometer scale control the optical properties of artificial structures. In a recent study of a gold bow-tie nanoantenna with variable feedback, the gap was tuned by nanomanipulation with an AFM tip and the optical resonances were measured with dark-field scattering spectroscopy.^[368]

We hope that this paper demonstrates that the field of force microscopy is very much alive, and new techniques and applications are developing rapidly. New material and environment combinations are being included into the realm of SPM high-resolution imaging on a regular basis. Combined with advances in the speed of scanning and chemical identification, the future will see many diverse fields and applications opened to this powerful suite of techniques.

Acknowledgements

We are grateful to Ezra Bussman, Jeppe Lauritsen and Alexander Schwarz for critical reading of the manuscript. This work was supported by the European COST program through Action D41. CB, ASF and CRH acknowledge support from the European Science Foundation through the FANAS network. ASF acknowledges support from the Academy of Finland through its Centre of Excellence program. ALS acknowledges support from the FP6 IP PICO-inside and from the Leverhulme Trust.

Received: June 23, 2010

Revised: August 20, 2010

Published online: November 11, 2010

- [1] E. Meyer, H. J. Hug, R. Bennewitz, *Scanning probe microscopy: the lab on a tip*, Springer-Verlag, Berlin, **2004**.
- [2] *Forces in scanning probe methods*, (Eds: H. J. Güntherodt, D. Anselmetti, E. Meyer), Springer-Verlag, Berlin **1995**.
- [3] L. Howald, H. Haefke, R. Lüthi, E. Meyer, G. Gerth, H. Rudin, H.-J. Güntherodt, *Phys. Rev. B* **1994**, *49*, 5651.
- [4] F. J. Giessibl, *Science* **1995**, *267*, 68.
- [5] F. J. Giessibl, *Rev. Mod. Phys.* **2003**, *75*, 949.
- [6] T. R. Albrecht, P. Grütter, D. Horne, D. Rugar, *J. Appl. Phys.* **1991**, *69*, 668.
- [7] R. García, R. Pérez, *Surf. Sci. Rep.* **2002**, *47*, 197.
- [8] *Noncontact Atomic Force Microscopy*, (Eds: S. Morita, R. Wiesendanger, E. Meyer) Springer, Berlin **2002**.
- [9] W. Hofer, A. S. Foster, A. L. Shluger, *Rev. Mod. Phys.* **2003**, *75*, 1287.
- [10] *Noncontact Atomic Force Microscopy Volume 2*, (Eds: S. Morita, F. J. Giessibl, R. Wiesendanger), Springer, Berlin **2010**.
- [11] L. Kelvin, G. Fitzgerald, W. Francis, *Philos. Mag. J. Sci.* **1898**, *46*, 82.
- [12] W. A. Zisman, *Rev. Sci. Instrum.* **1932**, *3*, 367.
- [13] G. Ertl, P. R. Norton, J. Rüstig, *Phys. Rev. Lett.* **1982**, *49*, 177.
- [14] S. Ladas, R. Imbihl, G. Ertl, *Surf. Sci.* **1989**, *219*, 88.
- [15] M. Schmidt, M. Nohlen, G. Bermes, M. Böhmer, K. Wandelt, *Rev. Sci. Instrum.* **1997**, *68*, 3866.
- [16] J. Fiasson, O. B. Harris, *J. Phys. E: Sci. Instrum.* **1977**, *10*, 1160.
- [17] L. B. Harris, J. Fiasson, *J. Phys. E: Sci. Instrum.* **1984**, *17*, 788.
- [18] L. B. Harris, J. Fiasson, *J. Phys. C: Solid State Phys.* **1985**, *18*, 4845.
- [19] L. B. Harris, *J. Phys. C: Solid State Phys.* **1987**, *20*, 5677.
- [20] G.-N. Luo, K. Yamaguchi, T. Terai, M. Yamawaki, *J. Alloys Compd.* **2003**, *349*, 211.
- [21] J. M. R. Weaver, D. W. Abraham, *J. Vac. Sci. Technol. B* **1991**, *9*, 1559.
- [22] M. Nonnenmacher, M. P. O. Boyle, H. K. Wickramasinghe, *Appl. Phys. Lett.* **1991**, *58*, 2921.
- [23] P. Girard, *Nanotechnology* **2001**, *12*, 485.
- [24] R. Berger, H. J. Butt, M. B. Retschke, S. A. L. Weber, *Macromol. Rapid Commun.* **2009**, *30*, 485.
- [25] A. S. Foster, W. A. Hofer, *Scanning Probe Microscopes: Atomic scale engineering by forces and currents*, Springer, Berlin **2006**.
- [26] D. A. Bonnell, *Probe Microscopy and Spectroscopy: Theory and Techniques and Applications*, Wiley-VCH, Berlin **2000**.
- [27] F. J. Giessibl, *Jpn. J. Appl. Phys.* **1994**, *33*, 3726.
- [28] R. A. Oliver, *Rep. Prog. Phys.* **2008**, *71*, 076501.
- [29] D. A. Bonnell, J. Garra, *Rep. Prog. Phys.* **2008**, *71*, 044501.
- [30] J. V. Lauritsen, M. Reichling, *J. Phys.: Condens. Matter* **2010**, *22*, 263001.
- [31] E. I. Altman, U. D. Schwarz, *Adv. Mater.* **2010**, *22*, 2854.
- [32] Y. Gan, *Surf. Sci. Rep.* **2009**, *64*, 99.
- [33] Ó. Custance, R. Pérez, S. Morita, *Nat. Nanotechnol.* **2009**, *4*, 803.
- [34] Y. Martin, C. C. Williams, H. K. Wickramasinghe, *J. Appl. Phys.* **1987**, *61*, 4723.
- [35] Q. Zhong, D. Inniss, K. Kjoller, V. B. Elings, *Surf. Sci. Lett.* **1993**, *290*, L688.
- [36] C. Barth, A. S. Foster, M. Reichling, A. L. Shluger, *J. Phys.: Condens. Matter* **2001**, *13*, 2061.
- [37] C. Barth, O. H. Pakarinen, A. S. Foster, C. R. Henry, *Nanotechnology* **2006**, *17*, S128.
- [38] H. Pakarinen, C. Barth, A. S. Foster, C. R. Henry, *J. Appl. Phys.* **2008**, *103*, 054313.
- [39] G. Couturier, R. Boisgard, D. Dietzel, J. P. Aimé, *Nanotechnology* **2005**, *16*, 1346.
- [40] R. J. Driscoll, M. G. Youngquist, J. D. Baleschwieler, *Nature* **1990**, *346*, 294.
- [41] F. Ohnesorge, G. Binnig, *Science* **1993**, *260*, 1451.
- [42] A. Engel, D. J. Müller, *Nat. Struct. Biol.* **2000**, *7*, 715.
- [43] K. D. Jandt, *Surf. Sci.* **2001**, *491*, 303.
- [44] P. J. James, M. Antognozzi, J. Tamayo, T. J. McMaster, J. M. Newton, M. J. Miles, *Langmuir* **2001**, *17*, 349.
- [45] T. Aoki, Y. Sowa, H. Yokota, M. Hiroshima, M. Tokunaga, Y. Ishii, T. Yanagida, *Single Mol.* **2001**, *2*, 183.
- [46] A. Philippssen, W. Im, A. Engel, T. Schirmer, B. Roux, D. J. Müller, *Biophys. J.* **2002**, *82*, 1667.
- [47] G. Kada, F. Kienberger, P. Hinterdorfer, *Nano Today* **2008**, *3*, 12.
- [48] D. J. Müller, Y. F. Dufrene, *Nat. Nanotechnol.* **2008**, *3*, 261.
- [49] F. J. Giessibl, H. Bielefeldt, S. Hembacher, J. Mannhart, *Appl. Surf. Sci.* **1999**, *140*, 352.
- [50] C. Barth, C. Claeys, C. R. Henry, *Rev. Sci. Instrum.* **2005**, *76*, 083907.
- [51] R. Bennewitz, M. Bammerlin, M. Guggisberg, C. Loppacher, A. Baratoff, E. Meyer, H.-J. Güntherodt, *Surf. Interface Anal.* **1999**, *27*, 462.
- [52] C. Barth, C. R. Henry, *Nanotechnology* **2006**, *17*, S155.
- [53] Y. Ma, A. S. Foster, R. M. Nieminen, *J. Chem. Phys.* **2005**, *122*, 144709.
- [54] M. A. Lantz, H. J. Hug, R. Hoffmann, S. Martin, A. Baratoff, H. J. Güntherodt, *Phys. Rev. B* **2003**, *68*, 035324.
- [55] H. Edwards, L. Taylor, W. Duncan, *J. Appl. Phys.* **1997**, *82*, 980.
- [56] F. J. Giessibl, *Appl. Phys. Lett.* **1998**, *73*, 3956.
- [57] T. Eguchi, Y. Hasegawa, *Phys. Rev. Lett.* **2002**, *89*, 266105.

- [58] F. J. Giessibl, S. Hembacher, H. Bielefeldt, J. Mannhart, *Science* **2000**, 289, 422.
- [59] S. M. Langkat, H. Hölscher, A. Schwarz, R. Wiesendanger, *Surf. Sci.* **2003**, 527, 12.
- [60] U. Kaiser, A. Schwarz, R. Wiesendanger, *Nature* **2007**, 446, 522.
- [61] M. Schmid, J. Mannhart, F. J. Giessibl, *Phys. Rev. B* **2008**, 77, 045402.
- [62] M. Ternes, C. P. Lutz, C. F. Hirjibehedin, F. J. Giessibl, A. J. Heinrich, *Science* **2008**, 319, 1066.
- [63] G. H. Simon, T. Koenig, M. Nilius, H. P. Rust, M. Heyde, H. J. Freund, *Phys. Rev. B* **2008**, 78, 113401.
- [64] L. Gross, F. Mohn, N. Moll, P. Liljeroth, G. Meyer, *Science* **2009**, 325, 1110.
- [65] L. Gross, F. Mohn, P. Liljeroth, J. Repp, F. J. Giessibl, G. Meyer, *Science* **2009**, 324, 1428.
- [66] M. Ara, A. Sasahara, H. Onishi, H. Tada, *Nanotechnology* **2004**, 15, S65.
- [67] D. Takamatsu, Y. Yamakoshi, K. Fukui, *J. Phys. Chem. B* **2006**, 110, 1968.
- [68] H. Dai, J. H. Hafner, A. G. Rinzler, D. T. Colbert, R. E. Smalley, *Nature* **1996**, 384, 147.
- [69] S. P. Jarvis, T. Uchihashi, T. Ishida, H. Tokumoto, Y. Nakayama, *J. Phys. Chem. B* **2000**, 104, 6091.
- [70] R. Wilson, V. Macpherson, *Nat. Nanotechnol.* **2009**, 4, 483.
- [71] A. I. Livshits, A. L. Shluger, A. Rohl, A. S. Foster, *Phys. Rev. B* **1999**, 59, 2436.
- [72] R. Pérez, M. C. Payne, I. Stich, K. Terakura, *Phys. Rev. Lett.* **1997**, 78, 678.
- [73] Y. Sugimoto, P. Pou, M. Abe, P. Jelinek, R. Pérez, S. Morita, Ó. Custance, *Nature* **2007**, 446, 64.
- [74] B. J. Albers, T. C. Schwendemann, M. Z. Baykara, N. Pilet, M. Liebmann, E. I. Altman, U. D. Schwarz, *Nat. Nanotechnol.* **2009**, 4, 307.
- [75] M. A. Lantz, H.-J. Hug, P. J. A. Schendel, R. Hoffmann, S. Martin, A. Baratoff, A. Abdurixit, H. J. Güntherodt, Ch. Gerber, *Phys. Rev. Lett.* **2000**, 84, 2642.
- [76] M. A. Lantz, H.-J. Hug, R. Hoffman, P. J. A. Schendel, P. Kappenberger, S. Martin, A. Baratoff, H.-J. Güntherodt, *Science* **2001**, 291, 2580.
- [77] P. Pou, S. A. Ghasemi, P. Jelinek, T. Lenosky, S. Goedecker, R. Perez, *Nanotechnology* **2009**, 20, 264015.
- [78] W. Allers, A. Schwarz, U. D. Schwarz, R. Wiesendanger, *Rev. Sci. Instrum.* **1998**, 69, 221.
- [79] H.-J. Hug, B. Stiefel, P. J. A. Schendel, A. Moser, S. Martin, H.-J. Güntherodt, *Rev. Sci. Instrum.* **1999**, 70, 3625.
- [80] R. Hoffmann, M. A. Lantz, H.-J. Hug, P. J. A. van Schendel, P. Kappenberger, S. Martin, A. Baratoff, H.-J. Güntherodt, *Phys. Rev. B* **2003**, 67, 085402.
- [81] R. Hoffmann, L. N. Kantorovich, A. Baratoff, H.-J. Hug, H.-J. Güntherodt, *Phys. Rev. Lett.* **2004**, 92, 146103.
- [82] R. Hoffmann, C. Barth, A. S. Foster, A. L. Shluger, H.-J. Hug, H.-J. Güntherodt, R. M. Nieminen, M. Reichling, *J. Am. Chem. Soc.* **2005**, 127, 17863.
- [83] M. Abe, Y. Sugimoto, Ó. Custance, S. Morita, *Appl. Phys. Lett.* **2005**, 87, 173503.
- [84] M. Abe, Y. Sugimoto, Ó. Custance, S. Morita, *Nanotechnology* **2005**, 16, 3029.
- [85] G. M. King, A. R. Carter, A. B. Churnside, L. S. Eberle, T. T. Perkins, *Nano Lett.* **2009**, 9, 1451.
- [86] T. Fukuma, Y. Ueda, S. Yoshioka, H. Asakawa, *Phys. Rev. Lett.* **2010**, 104, 016101.
- [87] H. Hölscher, S. M. Langkat, A. Schwarz, R. Wiesendanger, *Appl. Phys. Lett.* **2002**, 81, 4428.
- [88] M. Z. Baykara, T. C. Schwendemann, E. I. Altman, U. D. Schwarz, [89] N. Oyabu, P. Pou, Y. Sugimoto, P. Jelinek, M. Abe, S. Morita, R. Pérez, O. Custance, *Phys. Rev. Lett.* **2006**, 96, 106101.
- [90] C. Lazo, V. Caciuc, H. Hölscher, S. Heinze, *Phys. Rev. B* **2008**, 78, 214416.
- [91] K. I. Fukui, H. Onishi, Y. Iwasawa, *Chem. Phys. Lett.* **1997**, 280, 296.
- [92] M. Ashino, Y. Sugawara, S. Morita, M. Ishikawa, *Phys. Rev. Lett.* **2001**, 86, 4334.
- [93] S. Hembacher, F. Giessibl, J. Mannhart, C. Quate, *Phys. Rev. Lett.* **2005**, 94, 056101.
- [94] A. S. Foster, C. Barth, A. L. Shluger, M. Reichling, *Phys. Rev. Lett.* **2001**, 86, 2373.
- [95] A. S. Foster, C. Barth, A. L. Shluger, R. M. Nieminen, M. Reichling, *Phys. Rev. B* **2002**, 66, 235417.
- [96] Sh. Fujii, M. Fujihira, *Nanotechnology* **2006**, 17, S112.
- [97] S. Fujii, M. Fujihira, *Jpn. J. Appl. Phys.* **2006**, 45, 1986.
- [98] S. Hirth, F. Ostendorf, M. Reichling, *Nanotechnology* **2006**, 17, S148.
- [99] S. Fujii, M. Fujihira, *Nanotechnology* **2007**, 18, 084011.
- [100] A. S. Foster, T. Trevethan, A. L. Shluger, *Phys. Rev. B* **2009**, 80, 115421.
- [101] A. Klust, T. Ohta, A. Bostwick, Q. Yu, F. Ohuchi, M. Olmstead, *Phys. Rev. B* **2004**, 69, 035405.
- [102] J. Giessibl, M. Reichling, *Nanotechnology* **2005**, 16, S118.
- [103] S. Torbrügge, M. Reichling, A. Ishiyama, S. Morita, Ó. Custance, *Phys. Rev. Lett.* **2007**, 99, 56101.
- [104] S. Torbrügge, M. Cranney, M. Reichling, *Appl. Phys. Lett.* **2008**, 93, 073112.
- [105] K. Fukui, S. Takakusagi, R. Tero, M. Aizawa, Y. Namai, Y. Iwasawa, *Phys. Chem. Chem. Phys.* **2003**, 5, 5349.
- [106] S. Gritschneider, Y. Namai, Y. Iwasawa, M. Reichling, *Nanotechnology* **2005**, 16, S41.
- [107] S. Gritschneider, M. Reichling, *J. Phys. Chem. C* **2008**, 112, 2045.
- [108] S. Gritschneider, M. Reichling, *Nanotechnology* **2007**, 18, 044024.
- [109] S. Gritschneider, Y. Iwasawa, M. Reichling, *Nanotechnology* **2007**, 18, 044025.
- [110] C. Barth, C. R. Henry, *Phys. Rev. Lett.* **2003**, 91, 196102.
- [111] J. V. Lauritsen, M. C. R. Jensen, K. Venkataramani, B. Hinnemann, S. Helveg, B. S. Clausen, F. Besenbacher, *Phys. Rev. Lett.* **2009**, 103, 076103.
- [112] F. Ostendorf, C. Schmitz, S. Hirth, A. Kühnle, J. J. Kolodziej, M. Reichling, *Langmuir* **2009**, 25, 10764.
- [113] F. Ostendorf, S. Torbruegge, M. Reichling, *Phys. Rev. B* **2008**, 77, 041405.
- [114] E. Palacios-Lidon, O. Grauby, C. Henry, J. P. Astier, C. Barth, A. Baronnet, *Am. Mineral* **2010**, 95, 673.
- [115] M. Nimmrich, M. Kittelmann, P. Rahe, A. J. Mayne, G. Dujardin, A. von Schmidfeld, M. Reichling, W. Harneit, A. Kühnle, *Phys. Rev. B* **2010**, 81, 201403.
- [116] C. Barth, M. Reichling, *Nature* **2001**, 414, 54.
- [117] S. Torbruegge, F. Ostendorf, M. Reichling, *J. Phys. Chem. C* **2009**, 113, 4909.
- [118] F. Ostendorf, C. Schmitz, S. Hirth, A. Kühnle, J. J. Kolodziej, M. Reichling, *Nanotechnology* **2008**, 19, 305705.
- [119] J. Schütte, Ph. Rahe, L. Troeger, S. Rode, R. Bechstein, M. Reichling, A. Kühnle, *Langmuir* **2010**, 26, 8295.
- [120] M. Bammerlin, R. Lüthi, E. Meyer, J. Lü, M. Guggisberg, Ch. Loppacher, C. Gerber, H.-J. Güntherodt, *Appl. Phys. A* **1998**, 66, S293.
- [121] R. Bennewitz, A. S. Foster, L. N. Kantorovich, M. Bammerlin, Ch. Loppacher, S. Schär, M. Guggisberg, E. Meyer, A. L. Shluger, *Phys. Rev. B* **2000**, 62, 2074.
- [122] R. Bennewitz, O. Pfeiffer, S. Schär, V. Barwich, E. Meyer, L. N. Kantorovich, *Appl. Surf. Sci.* **2002**, 188, 232.
- [123] M. A. Cerda, J. Abad, A. Madgavkar, D. Martrou, S. Gauthier, *Nanotechnology* **2008**, 19, 045503.
- [124] F. Seitz, *Rev. Mod. Phys.* **1946**, 18, 384.

- [125] F. Seitz, *Rev. Mod. Phys.* **1954**, *26*, 7.
- [126] W. Hayes, A. M. Stoneham, *Defects and defect processes in nonmetallic solids*, Wiley-Interscience, New York **1985**.
- [127] L. N. Kantorovich, A. L. Shluger, A. M. Stoneham, *Phys. Rev. Lett.* **2000**, *85*, 3846.
- [128] H. E. Carrillo, H. A. Carrillo, O. J. Rubio, *Phys. Status Solidi* **1987**, *101*, 315.
- [129] K. Suzuki, *J. Phys. Soc. Jpn.* **1961**, *16*, 67.
- [130] C. J. J. Van Loon, D. J. W. Ijdo, *Acta Cryst. B* **1975**, *31*, 770.
- [131] M. Chall, B. Winkler, P. Blaha, K. Schwarz, *J. Phys. Chem. B* **2000**, *104*, 1191.
- [132] A. L. Guerrero, E. P. Butler, P. L. Pratt, L. W. Hobbs, *Philos. Mag. A* **1981**, *43*, 1359.
- [133] M. J. Yacamán, *Phys. Status Solidi B* **1973**, *56*, 429.
- [134] C. Barth, C. R. Henry, *New J. Phys.* **2009**, *11*, 043003.
- [135] C. Barth, C. R. Henry, *Phys. Rev. Lett.* **2008**, *100*, 96101.
- [136] A. S. Foster, C. Barth, C. R. Henry, *Phys. Rev. Lett.* **2009**, *102*, 256103.
- [137] G. A. Bassett, M. J. Yacamán, *Thin Solid Films* **1976**, *31*, 375.
- [138] P. Aceituno, F. Cussó, A. De Andrés, F. Jaque, *Solid State Commun.* **1984**, *49*, 209.
- [139] C. Cros, L. Hanebali, L. Latié, G. Villeneuve, W. Gang, *Solid State Ionics* **1983**, *9–10*, 139.
- [140] E. Lilley, J. B. Newkirk, *J. Mat. Sci.* **1967**, *2*, 567.
- [141] S. Kasper, J. S. Prenner, *Acta Cryst.* **1953**, *7*, 246.
- [142] P. Porta, G. Minelli, I. L. Botto, E. J. Baran, *J. Solid State Chem.* **1991**, *92*, 202.
- [143] C. R. Henry, *Surf. Sci. Rep.* **1998**, *31*, 231.
- [144] U. Heiz, U. Landman, *Nanocatalysis*, Springer Verlag, Berlin **2007**.
- [145] R. Bechstein, M. Kitta, J. Schütte, A. Kühnle, H. Onishi, *J. Phys. Chem. C* **2009**, *113*, 13199.
- [146] R. Bechstein, M. Kitta, J. Schütte, A. Kühnle, H. Onishi, *J. Phys. Chem. C* **2009**, *113*, 3277.
- [147] A. L. Linsebigler, G. Lu, J. T. Yates, *Chem. Rev.* **1995**, *95*, 735.
- [148] V. E. Henrich, P. A. Cox, *The Surface Science of Metal Oxides*, Cambridge University Press, Cambridge **1996**.
- [149] J. Lausmaa, *J. Electron Spectrosc. Relat. Phenom.* **1996**, *81*, 343.
- [150] J. Ni, K. H. Leung, Y. C. Leung, K. Sumathy, *Renewable Sustainable Energy Rev.* **2007**, *11*, 401.
- [151] U. Diebold, *Surf. Sci. Rep.* **2003**, *48*, 53.
- [152] U. Diebold, J. F. Anderson, K. O. Ng, D. Vanderbilt, *Phys. Rev. Lett.* **1996**, *77*, 1322.
- [153] K. I. Fukui, H. Onishi, Y. Iwasawa, *Phys. Rev. Lett.* **1997**, *79*, 4202.
- [154] M. Ashino, T. Uchihashi, K. Yokoyama, Y. Sugawara, S. Morita, M. Ishikawa, *Appl. Surf. Sci.* **2000**, *157*, 212.
- [155] S. H. Ke, T. Uda, K. Terakura, *Phys. Rev. B* **2002**, *65*, 125417.
- [156] A. S. Foster, O. H. Pakarinen, J. M. Airaksinen, J. D. Gale, R. M. Nieminen, *Phys. Rev. B* **2003**, *68*, 195410.
- [157] A. S. Foster, A. Y. Gal, J. M. Airaksinen, O. H. Pakarinen, Y. J. Lee, J. D. Gale, A. L. Shluger, R. M. Nieminen, *Phys. Rev. B* **2003**, *68*, 195420.
- [158] A. S. Foster, A. Y. Gal, J. D. Gale, Y. J. Lee, R. M. Nieminen, A. L. Shluger, *Phys. Rev. Lett.* **2004**, *92*, 036101.
- [159] J. V. Lauritsen, A. S. Foster, G. H. Olesen, M. C. Christensen, A. Kühnle, S. Helveg, J. R. Rostrup-Nielsen, B. S. Clausen, M. Reichling, F. Besenbacher, *Nanotechnology* **2006**, *17*, 3436.
- [160] S. Wendt, R. Schaub, J. Matthiesen, E. K. Vestergaard, E. Wahlström, M. D. Rasmussen, P. Thstrup, L. M. Molina, E. Lægsgaard, I. Stensgaard, B. Hammer, F. Besenbacher, *Surf. Sci.* **2005**, *598*, 226.
- [161] G. H. Enevoldsen, A. S. Foster, M. C. Christensen, J. V. Lauritsen, F. Besenbacher, *Phys. Rev. B* **2007**, *76*, 205415.
- [162] R. Bechstein, C. Schütte, J. Gonzalez, P. Jelinek, R. Perez, A. Kühnle, *Nanotechnology* **2009**, *20*, 505703.
- [163] G. H. Enevoldsen, H. P. Pinto, A. S. Foster, M. C. R. Jensen, A. Kühnle, M. Reichling, W. A. Hofer, J. V. Lauritsen, F. Besenbacher, *Phys. Rev. B* **2008**, *78*, 45416.
- [164] H. P. Pinto, H. Enevoldsen, F. Besenbacher, A. S. Foster, J. V. Lauritsen, *Nanotechnology* **2009**, *20*, 264020.
- [165] G. H. Enevoldsen, H. P. Pinto, A. S. Foster, M. C. R. Jensen, W. A. Hofer, B. Hammer, J. V. Lauritsen, F. Besenbacher, *Phys. Rev. Lett.* **2009**, *102*, 136103.
- [166] G. H. Enevoldsen, T. Glatzel, M. C. Christensen, J. V. Lauritsen, F. Besenbacher, *Phys. Rev. Lett.* **2008**, *100*, 236104.
- [167] J. Libuda, H.-J. Freund, *Surf. Sci. Rep.* **2005**, *57*, 157.
- [168] M. S. Chen, D. W. Goodman, *J. Phys.: Condens. Matter* **2008**, *20*, 264013.
- [169] M. E. Vaida, T. M. Bernhardt, C. Barth, F. Esch, U. Heiz, U. Landman, *Phys. Status Solidi B* **2010**, *247*, 1001.
- [170] J. Repp, S. Fölsch, G. Meyer, K. H. Rieder, *Phys. Rev. Lett.* **2001**, *86*, 252.
- [171] J. Repp, G. Meyer, F. E. Olsson, M. Persson, *Science* **2004**, *305*, 493.
- [172] M. Pivetta, F. Patthey, M. Stengel, A. Baldereschi, W.-D. Schneider, *Phys. Rev. B* **2005**, *72*, 115404.
- [173] J. Repp, G. Meyer, S. Paavilainen, F. E. Olsson, M. Persson, *Science* **2006**, *312*, 1196.
- [174] P. Liljeroth, J. Repp, G. Meyer, *Science* **2007**, *317*, 1203.
- [175] T. Filleter, W. Paul, R. Bennewitz, *Phys. Rev. B* **2008**, *77*, 8.
- [176] S. Schintke, S. Messerli, M. Pivetta, F. Patthey, L. Libiouille, M. Stengel, A. De Vita, W.-D. Schneider, *Phys. Rev. Lett.* **2001**, *87*, 276801.
- [177] M. Sterrer, M. Heyde, M. Novicki, N. Nilius, T. Risse, H. P. Rust, G. Pacchioni, H. J. Freund, *J. Phys. Chem. B* **2006**, *110*, 46.
- [178] M. Heyde, M. Sterrer, H. P. Rust, H.-J. Freund, *Appl. Phys. Lett.* **2005**, *87*, 083104.
- [179] M. Heyde, G. H. Simon, H. P. Rust, H.-J. Freund, *Appl. Phys. Lett.* **2006**, *89*, 263107.
- [180] M. Bielezki, T. Hynninen, T. M. Soini, M. Pivetta, C. R. Henry, A. S. Foster, F. Esch, C. Barth, U. Heiz, *Phys. Chem. Chem. Phys.* **2010**, *12*, 3203.
- [181] J. Libuda, F. Winkelmann, M. Bäumer, H.-J. Freund, T. Bertrams, H. Neddermeyer, K. Müller, *Surf. Sci.* **1994**, *318*, 61.
- [182] C. Becker, K. von Bergmann, A. Rosenhahn, J. Schneider, K. Wandelt, *Surf. Sci.* **2001**, *486*, L443.
- [183] M. Kulawik, N. Nilius, H. P. Rust, H.-J. Freund, *Phys. Rev. Lett.* **2003**, *91*, 256101.
- [184] G. Kresse, M. Schmid, E. Napetschnig, M. Shishkin, L. Kohler, P. Varga, *Science* **2005**, *308*, 1440.
- [185] G. H. Simon, T. König, H.-P. Rust, M. V. Ganduglia-Pirovano, J. Sauer, M. Heyde, H.-J. Freund, *Phys. Rev. B* **2010**, *81*, 073411.
- [186] G. Hamm, C. Becker, C. R. Henry, *Nanotechnology* **2006**, *17*, 1943.
- [187] A. Rosenhahn, J. Schneider, C. Becker, K. Wandelt, *J. Vac. Sci. Technol. A* **2000**, *18*, 1923.
- [188] G. Hamm, C. Barth, C. Becker, K. Wandelt, C. R. Henry, *Phys. Rev. Lett.* **2006**, *97*, 126106.
- [189] S. Gritschneider, C. Becker, K. Wandelt, M. Reichling, *J. Am. Chem. Soc.* **2007**, *129*, 4925.
- [190] H. Brune, M. Giovannini, K. Bromann, K. Kern, *Nature* **1998**, *394*, 451.
- [191] M. Schmid, G. Kresse, A. Buchsbaum, E. Napetschnig, S. Gritschneider, M. Reichling, P. Varga, *Phys. Rev. Lett.* **2007**, *99*, 196104.
- [192] M. Valden, X. Lai, D. W. Goodman, *Science* **1998**, *281*, 1647.
- [193] W. Mahoney, D. M. Schaefer, A. Patil, R. P. Andres, R. Reifengerger, *Surf. Sci.* **1994**, *316*, 383.
- [194] S. Kielbassa, A. Habich, J. Schnaidt, J. Bansmann, F. Weigl, H. G. Boyen, P. Ziemann, R. J. Behm, *Langmuir* **2006**, *22*, 7873.

- [195] C. Barth, C. R. Henry, *Appl. Phys. Lett.* **2006**, *89*, 252119.
- [196] C. Barth, C. R. Henry, *Nanotechnology* **2004**, *15*, 1264.
- [197] O. H. Pakarinen, C. Barth, A. S. Foster, R. M. Nieminen, C. R. Henry, *Phys. Rev. B* **2006**, *73*, 235428.
- [198] M. Goryl, F. Buatier de Mongeot, F. Krok, A. Vevecka-Priftaj, M. Szymonski, *Phys. Rev. B* **2007**, *76*, 75423.
- [199] J. M. Mativetsky, S. A. Burke, S. Fostner, P. Grütter, *Small* **2007**, *3*, 818.
- [200] J. M. Mativetsky, S. Fostner, S. A. Burke, P. Grütter, *Phys. Rev. B* **2009**, *80*, 045430.
- [201] T. Glatzel, L. Zimmerli, S. Koch, S. Kawai, E. Meyer, *Appl. Phys. Lett.* **2009**, *94*, 063303.
- [202] T. R. Ramachandran, C. Baur, A. Bugacov, A. Madhukar, B. E. Koel, A. Requicha, C. Gazen, *Nanotechnology* **1998**, *9*, 237.
- [203] R. Resch, A. Bugacov, C. Baur, B. E. Koel, A. Madhukar, A. A. G. Requicha, P. Will, *Appl. Phys. A* **1998**, *67*, 265.
- [204] K. Mougín, E. Gnecco, A. Rao, M. T. Cuberes, S. Jayaraman, E. W. McFarland, H. Haidara, E. Meyers, *Langmuir* **2008**, *24*, 1577.
- [205] M. Goryl, F. Krok, J. J. Kolodziej, P. Piatkowski, B. Such, M. Szymonski, *Vacuum* **2004**, *74*, 223.
- [206] G. Radu, D. Mautes, U. Hartmann, *J. Phys.: Conf. Ser.* **2007**, *61*, 966.
- [207] J. V. Zoval, R. M. Stiger, P. R. Biernacki, R. M. Penner, *J. Phys. Chem.* **1996**, *100*, 837.
- [208] T. Wenzel, J. Bosbach, F. Stietz, F. Träger, *Surf. Sci.* **1999**, *432*, 257.
- [209] C. Pang, H. Raza, S. A. Haycock, G. Thornton, *Surf. Sci.* **2000**, *460*, L510.
- [210] M. C. R. Jensen, K. Venkataramani, S. Helveg, M. R. Clausen, F. Besenbacher, J. V. Lauritsen, *J. Phys. Chem. C* **2008**, *112*, 16953.
- [211] S. L. Tait, L. T. Ngo, Q. Yu, S. C. Fain, C. T. Campbell, *J. Chem. Phys.* **2005**, *122*, 64712.
- [212] C. Barth, C. R. Henry, *J. Phys. Chem. C* **2009**, *113*, 247.
- [213] K. Venkataramani, S. Helveg, B. Hinnemann, M. Reichling, F. Besenbacher, J. V. Lauritsen, *Nanotechnology* **2010**, *21*, 265602.
- [214] Z. Gai, G. A. Farnan, J. P. Pierce, J. Shen, *Appl. Phys. Lett.* **2002**, *81*, 742.
- [215] Z. Gai, J. Y. Howe, J. Guo, D. A. Blom, E. W. Plummer, J. Shen, *Appl. Phys. Lett.* **2005**, *86*, 023107.
- [216] A. Klust, M. Grimsehl, J. Wollschläger, *Appl. Phys. Lett.* **2003**, *82*, 4483.
- [217] K. C. Lin, Y. H. Chiu, J. H. Lin, W. W. Pai, *Nanotechnology* **2005**, *16*, S63.
- [218] I. Yi, Y. Sugimoto, R. Nishi, M. Abe, S. Morita, *Nanotechnology* **2007**, *18*, 084013.
- [219] J. Colchero, O. Marti, J. Mlynek, A. Humbert, C. R. Henry, C. Chapon, *J. Vac. Sci. Technol. B* **1991**, *9*, 794.
- [220] R. Erlandsson, M. Eriksson, L. Olsson, U. Helmerson, I. Lundström, L. G. Petersson, *J. Vac. Sci. Technol. B* **1991**, *9*, 825.
- [221] C. Nie, T. Shimizu, H. Tokumoto, *J. Vac. Sci. Technol. B* **1994**, *12*, 1843.
- [222] D. Abriou, D. Gagnot, J. Jupille, F. Creuzet, *Surf. Rev. Lett.* **1998**, *5*, 387.
- [223] H. Fornander, J. Birch, P. Sandström, J. E. Sundgren, *Thin Solid Films* **1999**, *349*, 4.
- [224] G. Haas, A. Menck, H. Brune, J. V. Barth, J. A. Venables, K. Kern, *Phys. Rev. B* **2000**, *61*, 11105.
- [225] L. T. Hansen, A. Kühle, A. H. Sørensen, J. Bohr, P. E. Lindelof, *Nanotechnology* **1998**, *9*, 337.
- [226] M. Goryl, F. Mongeot, F. Krok, A. Vevecka-Priftaj, M. Szymonski, *Phys. Rev. B* **2007**, *76*, 075423.
- [227] J. Mativetsky, S. Fostner, S. Burke, P. Grütter, *Surf. Sci.* **2008**, *602*, L21.
- [228] S. C. Fain Jr., C. A. Polwarth, S. L. Tait, C. T. Campbell, R. H. French, *Nanotechnology* **2006**, *17*, S121.
- [229] J. Polesel-Mariss, H. Guo, T. Zambelli, S. Gauthier, *Nanotechnology* **2006**, *17*, 4204.
- [230] N. Nilius, *Surf. Sci. Rep.* **2009**, *64*, 595.
- [231] S. W. Hla, K.-H. Rieder, *Annu. Rev. Phys. Chem.* **2003**, *54*, 307.
- [232] M. L. Sushko, A. Y. Gal, M. Watkins, A. L. Shluger, *Nanotechnology* **2006**, *17*, 2062.
- [233] Ch. Loppacher, M. Bammerlin, M. Guggisberg, E. Meyer, H.-J. Güntherodt, R. Lüthi, R. Schlittler, J. K. Gimzewski, *Appl. Phys. A* **2001**, *72*, S105.
- [234] Ch. Loppacher, M. Guggisberg, O. Pfeiffer, E. Meyer, M. Bammerlin, R. Lüthi, R. Schlittler, J. K. Gimzewski, H. Tang, C. Joachim, *Phys. Rev. Lett.* **2003**, *90*, 066107.
- [235] D. Sawada, Y. Sugimoto, K. Morita, M. Abe, S. Morita, *Appl. Phys. Lett.* **2009**, *94*, 173117.
- [236] A. Sasahara, C. L. Pang, H. Onishi, *J. Phys. Chem. B* **2006**, *110*, 13453.
- [237] J. Schütte, R. Bechstein, M. Rohlfing, M. Reichling, A. Kühnle, *Phys. Rev. B* **2009**, *80*, 205421.
- [238] J. Schütte, R. Bechstein, P. Rahe, M. Rohlfing, A. Kühnle, H. Langhals, *Phys. Rev. B* **2009**, *79*, 045428.
- [239] P. Rahe, M. Nimmrich, A. Nefedov, M. Naboka, C. Wöll, A. Kühnle, *J. Phys. Chem. C* **2009**, *113*, 17471.
- [240] S. Frey, A. Schwarz, K. Lämmle, M. Prosen, R. Wiesendanger, *Nanotechnology* **2009**, *20*, 405608.
- [241] K. Lämmle, T. Trevethan, A. Schwarz, M. Watkins, A. L. Shluger, R. Wiesendanger, *Nano Lett.* **2010**, *10*, 2965.
- [242] B. Such, T. Trevethan, Th. Glatzel, S. Kawai, L. Zimmerli, E. Meyer, A. L. Shluger, C. H. M. Amijs, P. de Mendoza, A. M. Echavarren, *ACS Nano* **2010**, *4*, 277.
- [243] L. Bartels, G. Meyer, K.-H. Rieder, *Appl. Phys. Lett.* **1997**, *79*, 697.
- [244] L. Gross, F. Mohn, N. Moll, G. Meyer, R. Ebel, W. M. Abdel-Mageed, M. Jaspars, *Nat. Chem.* **2010**, *2*, 697.
- [245] A. S. Foster, A. Y. Gal, A. L. Shluger, R. M. Nieminen, *J. Phys. Chem.* **2005**, *109*, 4554.
- [246] P. Rahe, R. Bechstein, J. Schütte, F. Ostendorf, A. Kühnle, *Phys. Rev. B* **2008**, *77*, 195410.
- [247] N. Oyabu, Ó. Custance, I. Yi, Y. Sugawara, S. Morita, *Phys. Rev. Lett.* **2003**, *90*, 176102.
- [248] N. Oyabu, Y. Sugimoto, M. Abe, Ó. Custance, S. Morita, *Nanotechnology* **2005**, *16*, S112.
- [249] Y. Sugimoto, M. Abe, S. Hirayama, N. Oyabu, Ó. Custance, S. Morita, *Nat. Mater.* **2005**, *4*, 156.
- [250] M. B. Watkins, A. L. Shluger, *Phys. Rev. B* **2006**, *73*, 245435.
- [251] T. Trevethan, L. Kantorovich, J. Polesel-Mariss, S. Gauthier, A. L. Shluger, *Phys. Rev. B* **2007**, *76*, 085414.
- [252] T. Trevethan, M. Watkins, L. N. Kantorovich, A. L. Shluger, *Phys. Rev. Lett.* **2007**, *98*, 028101.
- [253] R. Nishi, D. Miyagawa, Y. Seino, I. Yi, S. Morita, *Nanotechnology* **2006**, *17*, S142.
- [254] J. N. Israelachvili, *Intermolecular and Surface Forces*, Academic Press, London **1991**.
- [255] G. Binnig, C. F. Quate, Ch. Gerber, *Phys. Rev. Lett.* **1986**, *56*, 930.
- [256] G. Binnig, C. Gerber, E. Stoll, T. R. Albrecht, C. F. Quate, *Europhys. Lett.* **1987**, *3*, 1281.
- [257] J. J. De Yoreo, L. A. Zepeda-Ruiz, R. W. Friddle, S. R. Qiu, L. E. Wasylenki, A. A. Chernov, G. H. Gilmer, P. M. Dove, *Cryst. Growth Des.* **2009**, *9*, 5135.
- [258] M. Egger, F. Ohnesorge, A. L. Weisenhorn, S. P. Heyn, B. Drake, C. B. Prater, S. A. C. Gould, P. K. Hansma, H. E. Gaub, *J. Struct. Biol.* **1990**, *103*, 89.
- [259] A. L. Weisenhorn, B. Drake, C. B. Prater, S. A. Gould, P. K. Hansma, F. Ohnesorge, M. Egger, S. P. Heyn, H. E. Gaub, *Biophys. J.* **1990**, *58*, 1251.
- [260] A. L. Weisenhorn, M. Egger, F. Ohnesorge, S. A. C. Gould, S. P. Heyn, H. G. Hansma, R. L. Sinsheimer, H. E. Gaub, P. K. Hansma, *Langmuir* **1991**, *7*, 8.
- [261] H. S. Quate, *Ultramicroscopy* **1992**, *42*, 1044.

- [262] H. Yamada, S. Okada, T. Fujii, M. Kageshima, A. Kawazu, H. Matsuda, H. Nakanishi, K. Nakayama, *Appl. Surf. Sci.* **1993**, *65*, 366.
- [263] G. A. Engel, *Biophys. J.* **1995**, *68*, 1681.
- [264] Q. Zhong, D. Inniss, K. Kjoller, V. B. Elings, *Surf. Sci.* **1993**, *290*, L688.
- [265] P. K. Hansma, J. P. Cleveland, M. Radmacher, D. A. Walters, P. E. Hillner, M. Bezanilla, M. Fritz, D. Vie, H. G. Hansma, C. B. Prater, C. B. Prater, *Appl. Phys. Lett.* **1994**, *64*, 1738.
- [266] J. Greve, *Appl. Phys. Lett.* **1994**, *64*, 2454.
- [267] D. Klinov, S. Magonov, *Appl. Phys. Lett.* **2004**, *84*, 2697.
- [268] P. Frederix, P. Bosshart, A. Engel, *Biophys. J.* **2009**, *96*, 329.
- [269] J. Tamayo, A. D. L. Humphris, M. J. Miles, *Appl. Phys. Lett.* **2000**, *77*, 582.
- [270] T. Fukuma, T. Ichii, K. Kobayashi, H. Yamada, K. Matsushige, *Appl. Phys. Lett.* **2005**, *86*, 034103.
- [271] A. Sasahara, S. Kitamura, H. Uetsuka, H. Onishi, *J. Phys. Chem. B* **2004**, *108*, 15735.
- [272] T. Fukuma, K. Kobayashi, K. Matsushige, H. Yamada, *Appl. Phys. Lett.* **2005**, *87*, 034101.
- [273] S. Rode, N. Oyabu, K. Kobayashi, H. Yamada, A. Kühnle, *Langmuir* **2009**, *25*, 2850.
- [274] T. Fukuma, M. J. Higgins, S. P. Jarvis, *Phys. Rev. Lett.* **2007**, *98*, 106101.
- [275] J. Giessibl, *Appl. Phys. Lett.* **2000**, *76*, 1470.
- [276] P. M. Hoffmann, S. Jeffery, J. B. Pethica, H. Özgür Özer, A. Oral, *Phys. Rev. Lett.* **2001**, *87*, 265502.
- [277] M. Heyde, M. Kulawik, H.-P. Rust, H.-J. Freund, *Phys. Rev. B* **2006**, *73*, 125320.
- [278] A. Bettac, J. Koeble, K. Winkler, B. Uder, M. Maier, A. Feltz, *Nanotechnology* **2009**, *20*, 264009.
- [279] M. Lee, B. Sung, N. Hashemi, W. Jhe, *Faraday Discuss.* **2009**, *141*, 415.
- [280] T. Uchihashi, M. Higgins, S. Yasuda, S. Jarvis, S. Akita, Y. Nakayama, J. E. Sader, *Appl. Phys. Lett.* **2004**, *85*, 3575.
- [281] T. Fukuma, K. Kobayashi, K. Matsushige, H. Yamada, *Appl. Phys. Lett.* **2005**, *86*, 193108.
- [282] B. Hoogenboom, H. Hug, Y. Pellmont, S. Martin, *Appl. Phys. Lett.* **2006**, *88*, 193109.
- [283] T. Fukuma, J. I. Kilpatrick, S. P. Jarvis, *Rev. Sci. Instrum.* **2006**, *77*, 123703.
- [284] O. Pfeiffer, R. Bennewitz, A. Baratoff, E. Meyer, P. Grütter, *Phys. Rev. B* **2002**, *65*, 161403.
- [285] M. Reinstadtler, U. Rabe, V. Scherer, U. Hartmann, A. Goldade, B. Bhushan, W. Arnold, *Appl. Phys. Lett.* **2003**, *82*, 2604.
- [286] N. Mullin, J. Hobbs, *Appl. Phys. Lett.* **2008**, *92*, 053103.
- [287] K. Voítchovsky, J. J. Kuna, S. A. Contera, E. Tosatti, F. Stellacci, *Nanotechnol.* **2010**, *5*, 401.
- [288] G. Hill, A. Rajagopal, A. Kahn, Y. Hu, *Appl. Phys. Lett.* **1998**, *73*, 662.
- [289] G. Butti, M. I. Trioni, H. Ishida, *Phys. Rev. B* **2004**, *70*, 195425.
- [290] L. Giordano, F. Cini, G. Pacchioni, *Phys. Rev. B* **2005**, *73*, 045414.
- [291] C. Zhang, B. Yoon, U. Landman, *J. Am. Chem. Soc.* **2007**, *129*, 2228.
- [292] S. Prada, U. Martinez, G. Pacchioni, *Phys. Rev. B* **2008**, *78*, 235423.
- [293] V. Palermo, M. Palma, P. Samori, *Adv. Mater.* **2006**, *18*, 145.
- [294] S. Kitamura, M. Iwatsuki, *Appl. Phys. Lett.* **1998**, *72*, 3154.
- [295] S. Kikukawa, S. Hosaka, R. Imura, *Rev. Sci. Instrum.* **1996**, *67*, 1463.
- [296] Th. Glatzel, S. Sadewasser, M. Ch. Lux-Steiner, *Appl. Surf. Sci.* **2003**, *210*, 84.
- [297] U. Zerweck, C. Loppacher, T. Otto, S. Grafström, L. M. Eng, *Phys. Rev. B* **2005**, *71*, 125424.
- [298] Y. Rosenwaks, R. Shikler, Th. Glatzel, S. Sadewasser, *Phys. Rev. B* **2004**, *70*, 085320.
- [299] E. B. Bussmann, N. Zheng, C. C. Williams, *Nano Lett.* **2006**, *6*, 2577.
- [300] C. Barth, C. R. Henry, *Phys. Rev. Lett.* **2007**, *98*, 136804.
- [301] T. Takahashi, T. Kawamukai, *Ultramicroscopy* **2000**, *82*, 63.
- [302] S. Sadewasser, M. Ch. Lux-Steiner, *Phys. Rev. Lett.* **2003**, *91*, 266101.
- [303] H. Diesinger, D. Deresmes, J. P. Nys, T. Melin, *Ultramicroscopy* **2008**, *108*, 773.
- [304] J. Lambert, G. de Loubens, C. Guthmann, M. Saint-Jean, T. Mélin, *Phys. Rev. B* **2005**, *71*, 155418.
- [305] C. Schönenberger, S. F. Alvarado, *Phys. Rev. Lett.* **1990**, *65*, 3162.
- [306] N. Felidj, J. Lambert, C. Guthmann, M. Saint Jean, *Eur. Phys. J.: Appl. Phys.* **2000**, *12*, 85.
- [307] J. M. Sturm, A. I. Zinine, H. Wormeester, B. Poelsema, R. G. Bankras, J. Holleman, J. Schmitz, *J. Appl. Phys.* **2005**, *97*, 063709.
- [308] P. M. Bridger, Z. Z. Bandić, E. C. Piquette, T. C. McGill, *Appl. Phys. Lett.* **1999**, *74*, 3522.
- [309] C. Schönenberger, *Phys. Rev. B* **1992**, *45*, 3861.
- [310] T. Mélin, H. Diesinger, D. Deresmes, D. Stiévenard, *Phys. Rev. Lett.* **2004**, *92*, 166101.
- [311] R. Dianoux, H. J. H. Smilde, F. Marchi, N. Buffet, P. Mur, F. Comin, J. Chevrier, *Phys. Rev. B* **2005**, *71*, 125303.
- [312] J. Nishitani, K. Makihara, M. Ikeda, H. Murakami, S. Higashi, S. Miyazaki, *Thin Solid Films* **2006**, *508*, 190.
- [313] H. Diesinger, T. Melin, S. Barbet, D. Deresmes, D. Stiévenard, *Phys. Status Solidi A* **2006**, *203*, 1344.
- [314] E. Bussmann, C. C. Williams, *Appl. Phys. Lett.* **2006**, *88*, 263108.
- [315] D. Ochs, W. Maus-Friedrichs, M. Brause, J. Günster, V. Kempter, V. Puchin, A. L. Shluger, L. N. Kantorovich, *Surf. Sci.* **1996**, *365*, 557.
- [316] S. Krischok, P. Stracke, V. Kempter, *Appl. Phys. A* **2006**, *82*, 167.
- [317] M. E. Vaida, T. Gleitsmann, R. Tchitnga, T. M. Bernhardt, *J. Phys. Chem. C* **2009**, *113*, 10264.
- [318] B. Yoon, H. Häkkinen, U. Landman, A. S. Antonietti, J.-M. Wörz, S. Abbet, K. Judai, U. Heiz, *Science* **2005**, *307*, 403.
- [319] Ch. Loppacher, U. Zerweck, L. M. Eng, *Nanotechnology* **2004**, *15*, 9.
- [320] Th. Glatzel, L. Zimmerli, S. Koch, B. Such, S. Kawai, E. Meyer, *Nanotechnology* **2009**, *20*, 264016.
- [321] Ch. Loppacher, U. Zerweck, L. M. Eng, S. Seifert, G. Gemming, C. Olbrich, K. Morawetz, M. Schreiber, *Nanotechnology* **2006**, *17*, 1568.
- [322] F. Krok, J. J. Kolodziej, B. Such, P. Czuba, P. Struski, P. Piatkowski, M. Szymonski, *Surf. Sci.* **2004**, *566*, 63.
- [323] F. Krok, K. Sajewicz, J. Konior, M. Goryl, P. Piatkowski, M. Szymonski, *Phys. Rev. B* **2008**, *77*, 235427.
- [324] C. Barth, T. Hynninen, M. Bielecki, C. R. Henry, A. S. Foster, F. Esch, U. Heiz, *New J. Phys.* **2010**, *12*, 093024.
- [325] U. Zerweck, C. Loppacher, L. M. Eng, *Nanotechnology* **2006**, *17*, S107.
- [326] J. Chen, *Introduction to scanning tunneling microscopy*, Oxford University Press, Oxford **1993**.
- [327] R. Wiesendanger, *Scanning probe microscopy and spectroscopy: Methods and applications*, Cambridge University Press, Cambridge **1994**.
- [328] D. Ricci, G. Pacchioni, P. V. Shluger, A. L. Sushko, *Surf. Sci.* **2003**, *542*, 293.
- [329] Ch. Sommerhalter, T. W. Matthes, Th. Glatzel, A. Jäger-Waldau, M. Ch. Lux-Steiner, *Appl. Phys. Lett.* **1999**, *75*, 286.
- [330] R. Ludeke, E. Cartier, *Appl. Phys. Lett.* **2001**, *78*, 3998.
- [331] Th. Glatzel, S. Sadewasser, R. Shikler, Y. Rosenwaks, M. Ch. Lux-Steiner, *Mater. Sci. Eng. B* **2003**, *102*, 138.
- [332] S. Ogawa, S. Ichikawa, *Phys. Rev. B* **1995**, *51*, 17231.

- [333] L. Pang, T. V. Ashworth, H. Raza, S. A. Haycock, G. Thornton, *Nanotechnology* **2004**, *15*, 862.
- [334] Y. Frenkel, *Kinetic theory of liquids*, The Clarendon Press, Oxford **1946**.
- [335] R. W. Whitworth, *Adv. Phys.* **1975**, *24*, 203.
- [336] K. L. Kliewer, J. S. Koehler, *Phys. Rev.* **1965**, *140*, A1226.
- [337] K. L. Kliewer, *Phys. Rev.* **1965**, *140*, A1241.
- [338] K. Kliewer, *J. Phys. Chem. Solids* **1966**, *27*, 705.
- [339] R. B. Poepfel, J. M. Blakely, *Surf. Sci.* **1969**, *15*, 507.
- [340] R. C. Baetzold, *Phys. Rev. B* **1995**, *52*, 11424.
- [341] P. Egberts, T. Filleter, R. Bennewitz, *Nanotechnology* **2009**, *20*, 264005.
- [342] L. N. Kantorovich, J. M. Holender, M. J. Gillan, *Surf. Sci.* **1995**, *343*, 221.
- [343] E. Scorza, U. Birkenheuer, C. Pisani, *J. Chem. Phys.* **1997**, *107*, 9645.
- [344] L. J. Klein, C. C. Williams, *Appl. Phys. Lett.* **2001**, *79*, 1828.
- [345] F. Bocquet, L. Nony, Ch. Loppacher, Th. Glatzel, *Phys. Rev. B* **2008**, *78*, 035410.
- [346] L. Nony, F. Bocquet, C. Loppacher, Th. Glatzel, *Nanotechnology* **2009**, *20*, 264014.
- [347] L. Nony, A. S. Foster, F. Bocquet, Ch. Loppacher, *Phys. Rev. Lett.* **2009**, *103*, 036802.
- [348] G. H. Enevoldsen, Th. Glatzel, M. C. Christensen, J. V. Lauritsen, F. Besenbacher, *Phys. Rev. Lett.* **2008**, *100*, 236104.
- [349] S. Sadewasser, P. Jelinek, C. K. Fang, O. Yamada, Y. Custance, Y. Sugimoto, M. Abe, S. Morita, *Phys. Rev. Lett.* **2009**, *103*, 266103.
- [350] A. Sinensky, A. Belcher, *Nat. Nanotechnol.* **2007**, *2*, 653.
- [351] T. Hallam, M. Lee, N. Zhao, I. Nandhakumar, M. Kemerink, M. Heeney, I. McCulloch, H. Sirringhaus, *Phys. Rev. Lett.* **2009**, *103*, 256803.
- [352] M. Haruta, *Catal. Today* **1997**, *36*, 153.
- [353] M. Sterrer, T. Risse, M. Heyde, H.-P. Rust, H.-J. Freund, *Phys. Rev. Lett.* **2007**, *98*, 206103.
- [354] C. Harding, V. Habibpour, S. Kunz, A. N. S. Farnbacher, U. Heiz, B. Yoon, U. Landman, *J. Am. Chem. Soc.* **2009**, *131*, 538.
- [355] W. A. de Heer, *Rev. Mod. Phys.* **1993**, *65*, 611.
- [356] S. J. Wang, G. Cheng, X. H. Jiang, Y. C. Li, Y. B. Huang, Z. L. Du, *Appl. Phys. Lett.* **2006**, *88*, 212108.
- [357] K. Makihara, J. Xu, M. Ikeda, H. Murakami, S. Higashi, S. Miyazaki, *Thin Solid Films* **2006**, *508*, 186.
- [358] M. Schnippering, M. Carrara, A. Foelske, R. Fermín, D. J. Kötz, *Phys. Chem. Chem. Phys.* **2007**, *9*, 725.
- [359] N. Ferralis, R. Maboudian, C. Carraro, *J. Phys. Chem. C* **2007**, *111*, 7508.
- [360] K. Hiehata, A. Sasahara, H. Onishi, *Nanotechnology* **2007**, *18*, 084007.
- [361] C. Barth, E. Palacios-Lidon, C. R. Henry, unpublished.
- [362] L. M. Picco, L. Bozec, A. Ulcinas, D. J. Antognozzi, M. Engledew, M. A. Horton, M. J. Miles, *Nanotechnology* **2007**, *18*, 44030.
- [363] Z. Stieg, H. I. Rasool, J. K. Gimzewski, *Rev. Sci. Instrum.* **2008**, *79*, 103701.
- [364] A. Anne, C. Demaille, C. Goyer, *ACS Nano* **2009**, *3*, 819.
- [365] E. Bailo, V. Deckert, *Chem. Soc. Rev.* **2008**, *37*, 921.
- [366] E. Bailo, V. Deckert, *Angew. Chem. Int. Ed.* **2008**, *47*, 1658.
- [367] G. Benstetter, R. Bib Berger, D. Liu, *Thin Solid Films* **2009**, *517*, 5100.
- [368] J. Merlein, M. Kahl, A. Zuschlag, A. Sell, A. Boneberg, J. Halm, P. Leiderer, A. Leitenstorfer, R. Brat, *Nat. Photonics* **2008**, *2*, 230.
- [369] E. Meyer, *Prog. Surf. Sci.* **1992**, *41*, 3.
- [370] B. D. Terris, J. E. Stern, D. Rugar, H. J. Mamin, *J. Vac. Sci. Technol. A* **1990**, *8*, 374.
- [371] C. Guillemot, P. Budau, J. Chevrier, F. Marchi, F. Comin, C. Alandi, F. Bertin, N. Buffet, C. Wyon, P. Mur, *Europhys. Lett.* **2002**, *59*, 566.
- [372] J. E. Stern, B. D. Terris, H. J. Mamin, D. Rugar, *Appl. Phys. Lett.* **1988**, *53*, 2717.
- [373] P. Girard, M. Ramonda, D. Saluel, *J. Vac. Sci. Technol. B* **2002**, *20*, 1348.
- [374] B. D. Terris, J. E. Stern, D. Rugar, H. J. Mamin, *Phys. Rev. Lett.* **1989**, *63*, 2669.
- [375] P. Girard, G. C. Solal, S. Belaidi, *Microelectron. Eng.* **1996**, *31*, 215.
- [376] F. Müller, A. D. Müller, M. Hietschold, S. Kammer, *Meas. Sci. Technol.* **1998**, *9*, 734.
- [377] M. Luna, F. Rieutord, N. A. Melman, Q. Dai, M. Salmeron, *J. Phys. Chem. A* **1998**, *102*, 6793.
- [378] S. Ghosal, A. Verdaguer, J. C. Hemminger, M. Salmeron, *J. Phys. Chem. A* **2005**, *109*, 4744.
- [379] M. Luna, D. F. Ogletree, M. Salmeron, *Nanotechnology* **2006**, *17*, S178.
- [380] E. Bussmann, D. J. Kim, C. C. Williams, *Appl. Phys. Lett.* **2004**, *85*, 2538.
- [381] M. Sterrer, T. Risse, U. M. Pozzoni, L. Giordano, M. Heyde, H. P. Rust, G. Pacchioni, H.-J. Freund, *Phys. Rev. Lett.* **2007**, *98*, 096107.